Measurement Notes

Note 45

October 1993

BALUNS
for
DRIVING HIGH POWER LEVELS
from
50 OHM AMPLIFIERS/CABLES
into
HIGH IMPEDANCE ANTENNAS/LOADS

Gary D. Sower
EG&G Special Projects
Albuquerque, NM 87106

ABSTRACT

A **BALUN** is a special type of transformer for converting a **BAL**anced signal to an **UN**balanced signal (or a **BAL**ancing **UN**it). By reprocity, it can also convert the unbalanced signal into a balanced signal; by convention it retains the same name in this applicatin. High-frequency, broad-band baluns can be constructed with transmission lines. In such construction, the turns ratio is limited to the ratio of small integers, such as 2:1. The transformed impedance ratio is the square of the turns ratio, such as 4:1. The balun can be driven from the unbalanced side to give a balanced output of some multiple of the input impedance. Power levels of hundreds of watts can be driven into balanced loads (antennas) with a properly designed balun.

We consider here the case of a driver balun which is constructed from a pair of coaxial cables (Dual Coaxial Balun) which are wired in parallel at the input and form a series output connection across the load (antenna). The characteristic impedance of the required coax is twice the source impedance and half of the impedance of a matched load. For a 50 ohm source, the coax must be 100 ohms and the matched load 200 ohms; unmatched loads of varying impedance, such as an antenna, can be driven with a resulting loss of power due to the impedance mismatch.

The series output is obtained by isolation of the output from the input of the balun: currents must be prevented from travelling on the exterior of the coaxial cables. This is usually done with ferrite beads, which act as high-frequency chokes. The normal "back impedance" from an isolated coax shield to the external world is 200-300 ohms. When the coax is inside another conductor such as the housing of a balun, the back impedance is that of the transmission line so formed. This is often of the same magnitude or lower than the impedance of the load being driven, which significantly perturbs the signal driven onto the antenna. The ferrite beads will greatly increase this back impedance, allowing more power to be transferred to the antenna. Some power will still be transmitted into the ferrite bead transmission line, robbing from the antenna signal. This power is absorbed by the ferrite in the form of heat, raising its

temperature, which in some cases be large enough to exceed the Curie temperature of the ferrite, causing erratic performance or failure of the balun.

The key to building a successful high power driver balun is to make the back impedance of the coaxial cables used within the balun large with respect to the load impedance. This is done by maximizing both the characteristic impedance of the transmission line formed between the coax shields and the balun housing, and the wave impedance of the ferrite with which it is loaded.

I. DUAL COAXIAL BALUN (DCB-1) EQUIVALENT CIRCUIT

Impedance matching networks, known as baluns, are used in electromagnetic simulation antennas to improve the power transfer between a low-impedance power amplifier and a high-impedance antenna. The baluns described in this paper are specifically designed to drive the Ellipticus antenna [1], [2], [3], [4]. The **Dual Coaxial Balun (DCB-1)** [5] is intended as a "low-frequency" driver, covering the frequency band from 300 kHz to 1000 MHz (1 GHz). The **Balantenna** [6] is intended for high-frequency applications, from one GHz to as high in frequency as possible. Both baluns are for use with power amplifiers of 200 Watts.

The "back impedance" Z_B may be that of a coaxial structure, such as that between the positive output coax and the tubular housing of the DCB-1, or that of a biconical structure as in the Balantenna , or some other transmission line structure.

The structure of the **DCB-1** forms a transmission line of characteristic impedance between the **outside** of the positive (non-inverting) coaxial cable and the inside of the metal tube of the balun housing, as shown in **Figure 1**. The outside of the negative (inverting) cable is topologically equivalent to the housing (local ground).

The input of the ferrite-loaded transmission line presents the back characteristic impedance Z_B which appears in addition to the output load impedance of the antenna. The back impedance is electrically located between the output of the positive cable shield and ground, as seen in **Figure 2.**

The load impedance seen by the positive output cable, top in the figure, is the antenna impedance in series with the parallel combination of the back impedance and the characteristic impedance of the other cable, **Figure 3**:

$$Z_1 = Z_A + \frac{Z_B Z_C}{Z_B + Z_C} . \qquad (1)$$

This presents a reflection coefficient to an incident signal from the coax:

$$\rho_1 = \frac{Z_1 - Z_C}{Z_1 + Z_C} = \frac{Z_A Z_B + Z_A Z_C - Z_C^2}{Z_A Z_B + Z_A Z_C + 2 Z_B Z_C + Z_C^2} . \qquad (2)$$

The load impedance seen by the negative output cable (bottom) is the back impedance in parallel with the series combination of the antenna impedance and the characteristic impedance of the other cable **Figure 4**:

$$Z_2 = \frac{Z_B (Z_A + Z_C)}{Z_A + Z_B + Z_C} . \qquad (3)$$

This load impedancegives a reflection coefficient of:

$$\rho_2 = \frac{Z_2 - Z_C}{Z_2 + Z_C} = \frac{Z_A Z_B - Z_A Z_C - Z_C^2}{Z_A Z_B + Z_A Z_C + 2 Z_B Z_C + Z_C^2} . \qquad (4)$$

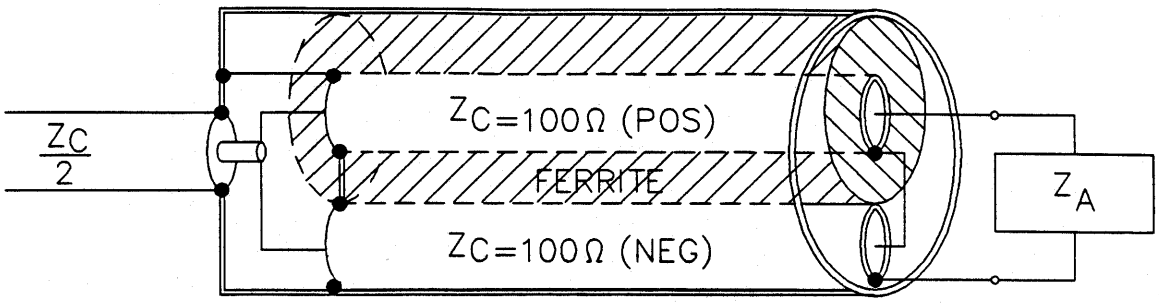

Figure 1. Balun Circuit Configuration.

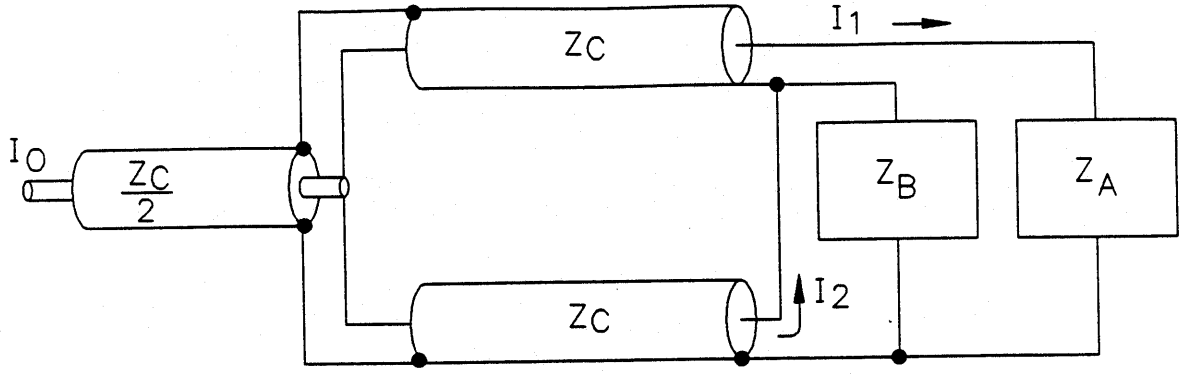

Figure 2. Balun Equivalent Circuit.

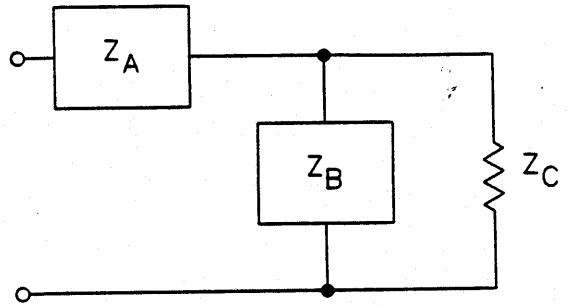

Figure 3. Load Impedance seen by Output of Positive Cable.

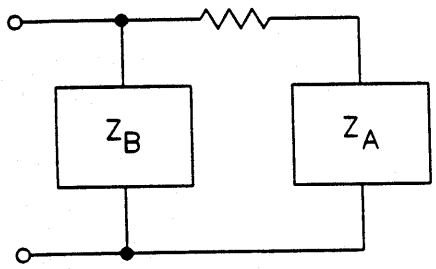

Figure 4. Load Impedance seen by Output of Negative Cable.

Initial Input Signal: The transmitted current out of the positive cable and into the antenna is:

$$I_T^P = \frac{I_0}{2}(1 - \rho_1) . \tag{5}$$

The current transmitted into the ferrite-loaded back impedance is:

$$I_B^P = I_T^P \left(\frac{Z_C}{Z_B + Z_C} \right), \tag{6}$$

and that into the other cable is:

$$I_C^P = I_T^P \left(\frac{Z_B}{Z_B + Z_C} \right) = \frac{I_0}{2}(\Gamma_1) . \tag{7}$$

A new variable is defined as:

$$\Gamma_1 = (1 - \rho_1) \left(\frac{Z_B}{Z_B + Z_C} \right) . \tag{8}$$

The transmitted current out of the negative cable is:

$$I_T^N = \frac{I_0}{2}(1 - \rho_2) . \tag{9}$$

The part of this that goes into the back impedance is:

$$I_B^N = I_T^N \left(\frac{Z_2}{Z_B} \right) = I_T^N \left(\frac{Z_A + Z_C}{Z_A + Z_B + Z_C} \right) . \tag{10}$$

The part that goes into the positive cable and into the antenna is:

$$I_A^N = I_C^N = I_T^N \left(\frac{Z_B}{Z_A + Z_B + Z_C} \right) \equiv \frac{I_0}{2}(\Gamma_2) , \tag{11}$$

where a new variable is defined as:

$$\Gamma_2 = (1 - \rho_2) \left(\frac{Z_B}{Z_A + Z_B + Z_C} \right) . \tag{12}$$

The two components of the current into the antenna are in phase, so the total current into the antenna, by linear superposition, is the sum of equations **(5)** and **(11)**:

$$I_A = I_T^P + I_A^N = \frac{I_0}{2}(\Gamma_2 + 1 - \rho_1) . \quad (13)$$

The two components of the current into the back impedance are out of phase, so the total current is the difference between equations **(6)** and **(10)**:

$$I_B = I_T^P \left(\frac{Z_C}{Z_B + Z_C} \right) - I_T^N \left(\frac{Z_A + Z_C}{Z_A + Z_B + Z_C} \right) . \quad (14)$$

The reflected current back into the first cable is:

$$I_R^P = \frac{I_0}{2}(- \rho_1) . \quad (15)$$

The reflected current back into the second cable is:

$$I_R^N = \frac{I_0}{2}(- \rho_2) . \quad (16)$$

The total return current back into the positive cable is the sum of equations **(11)** and **(15)**:

$$R^P = \frac{I_0}{2}(\Gamma_2 - \rho_1) . \quad (17)$$

The total current back into the negative cable is the sum of equations **(7)** and **(16)**:

$$R^N = \frac{I_0}{2}(\Gamma_1 - \rho_2) . \quad (18)$$

Multiple Reflections in Balun: The above discussion is applicable for the case where the currents back into the two cables are terminated in their characteristic impedance. In actuality, each of these 100 ohm cables sees an impedance at the "T" joint of the input 50 ohm cable in parallel with the other 100 ohm output cable, resulting in a load impedance at this point of 33⅓ ohms. This gives a reflection coefficient for the backward signals of :

$$\rho_T = -0.5 . \quad (19)$$

Multiple reflections occur on the 100 ohm cables because of the impedance discontinuities at both ends of them. One way to track the reflections and transmissions with such a system is by means of a **bounce diagram** as in **Figure 5**. The input line is on the left, the pair of 100 ohm coaxial cables in the middle, and the load impedances on the right. Time, and the successive signals, progress from the top to the bottom of the diagram.

The input signal from the source on the 50 ohm cable sees the two 100 ohm cables in parallel at the first boundary, which gives a matched load of 50 ohms at this point and no reflection.

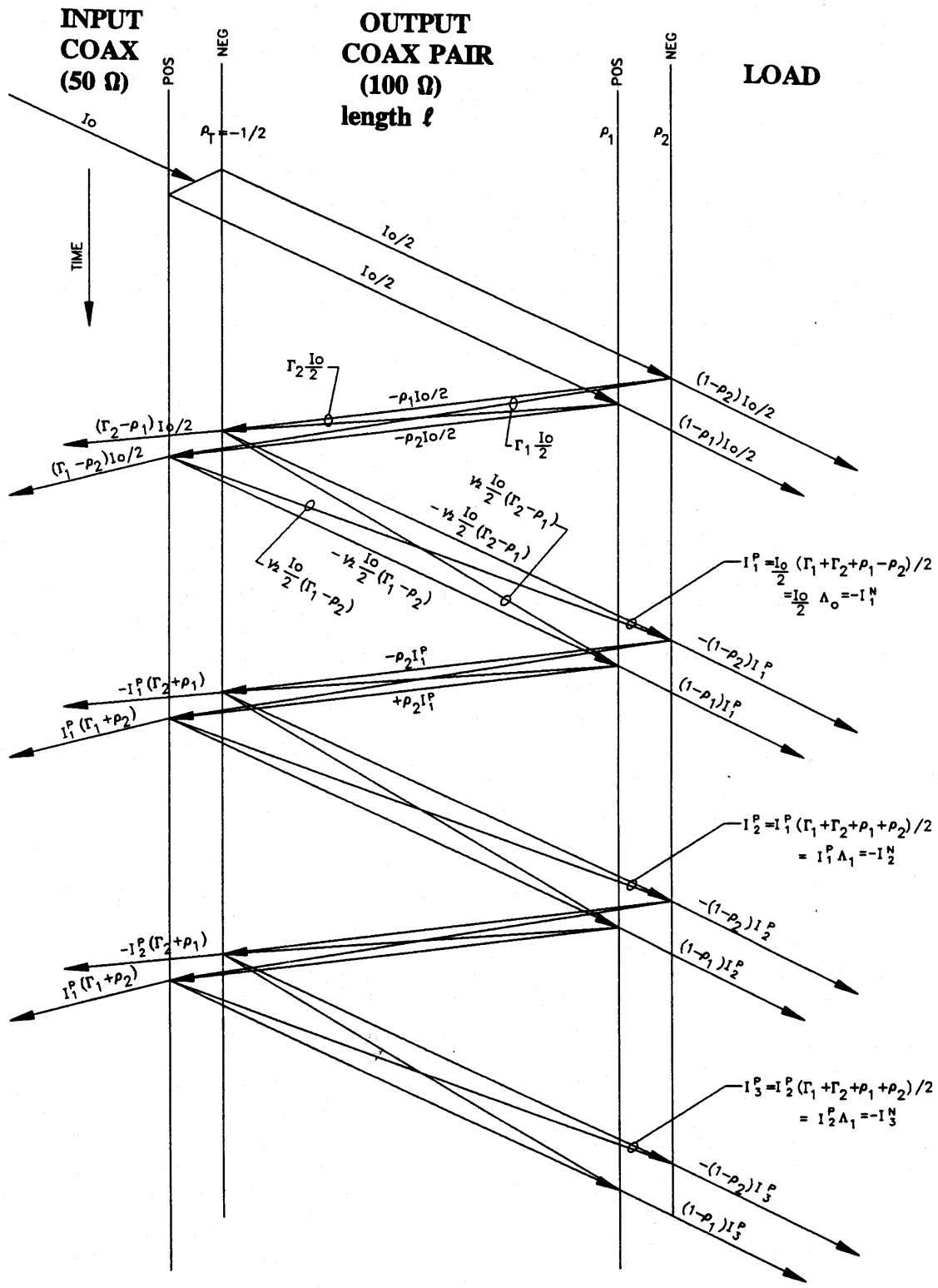

Figure 5. Bounce Diagram for Multiple Reflections in DCB-1.

The two 100 ohm cables are shown as two lines on the diagram. In actuality, the timing of their outputs is identical, so they really occur at the same point in time on the right side of the diagram, but physically separated. The reflections from each of these cables back into itself are also shown as solid lines. The signals coupling across from the other cables are shown as dashed lines. These are schematically shown to converge in the actual cable at the other side of the diagram.

The reflection coefficients at the outputs of the cables are given above in equations **(2)** and **(4)** for the positive and negative outputs, respectively. These reflection coefficients and their associated transmission coefficients are the same for the initial signal and all subsequent bounced signals.

The total reverse-propagating signal R_i on each cable are thus given by equations **(17)** and **(18)**, with the incident currents for each bounce I_i replacing the incident values of $I_0/2$:

$$R_i^P = I_i^P(\Gamma_2 - \rho_1) , \tag{20}$$

$$R_i^N = I_i^N(\Gamma_1 - \rho_2) . \tag{21}$$

The reflection coefficient for each signal component at the "T" joint is the same, given by equation **(19)**. The reflected current on each cable is the incident current **(20)** or **(21)** times the negative of **(19)**. The current transmitted into the 33⅓ load from each cable is 1.5 times that of **(20)** or **(21)**, of which one-third goes into the other 100 ohm cable and two-thirds into the 50 ohm source cable. The signals transmitted to the other cable are out of phase with respect to the self-reflected signals, so the signals going back toward the output load from the first bounce are:

$$I_1^P = \frac{I_0}{2}\,\frac{1}{2}(\Gamma_1 - \Gamma_2 + \rho_1 - \rho_2)\, e^{-jk2\ell} = \frac{I_0}{2}\Lambda_0 , \tag{22}$$

$$I_1^N = -\frac{I_0}{2}\,\frac{1}{2}(\Gamma_1 - \Gamma_2 + \rho_1 - \rho_2)\, e^{-jk2\ell} = -\frac{I_0}{2}\Lambda_0 = -I_1^P . \tag{23}$$

The exponential factor is the phase difference for the two-way propagation over the 100 ohm cables of length ℓ and wave number k, and a new variable is defined as:

$$\Lambda_0 = \frac{1}{2}(\Gamma_1 - \Gamma_2 + \rho_1 - \rho_2)\, e^{-jk2\ell} . \tag{24}$$

The next reflections at the cable outputs give:

$$R_2^P = I_1^N\Gamma_2 - I_1^P\rho_1 = -I_1^P(\Gamma_2 + \rho_1) , \tag{25}$$

$$R_2^N = I_1^P\Gamma_1 - I_1^N\rho_2 = I_1^P(\Gamma_1 + \rho_2) . \tag{26}$$

The reflections and transmissions from the cable inputs then give:

$$I_2^P = \left[I_1^P \frac{1}{2}(\Gamma_2 + \rho_1) - I_1^N \frac{1}{2}(\Gamma_1 + \rho_2) \right] e^{-jk2\ell} = I_1^P \Lambda_1 = -I_2^N , \tag{27}$$

with the new variable:

$$\Lambda_1 = \frac{1}{2}(\Gamma_1 + \Gamma_2 + \rho_1 + \rho_2)\, e^{-jk2\ell} . \tag{28}$$

For all successive bounces, it is apparent that:

$$I_i^P = I_{i-1}^P \Lambda_1 = -I_i^N . \tag{29}$$

The total incident current at the output of the positive cable is the sum of the initial current plus all of the bounces:

$$I^P = \frac{I_0}{2} + \sum_{i=1}^{\infty} I_i^P . \tag{30}$$

This can be expanded and simplified to give:

$$I^P = \frac{I_0}{2} + \frac{I_0}{2}\Lambda_0\left(1 + \Lambda_1 + \Lambda_1^2 + \Lambda_1^3 + \Lambda_1^4 + \cdots\right) = \frac{I_0}{2}\left[1 + \frac{\Lambda_0}{1 - \Lambda_1}\right] . \tag{31}$$

Similarly, the total incident current at the output of the negative cable is :

$$I^N = \frac{I_0}{2} + \sum_{i=1}^{\infty} I_i^N = \frac{I_0}{2}\left[1 - \frac{\Lambda_0}{1 - \Lambda_1}\right] . \tag{32}$$

Equation (12) can now be modified to give the total current into the antenna:

$$I_A = I^P + I^N\left(\frac{Z_B}{Z_A + Z_B + Z_C}\right) .$$

Likewise, the total current into the ferrite back impedance is, from equation (13):

$$I_B = I^P\left(\frac{Z_C}{Z_B + Z_C}\right) - I^N\left(\frac{Z_A + Z_C}{Z_A + Z_B + Z_C}\right) .$$

The total current lost back into the 50 ohm source cable (presumably reverse terminated in its characteristic impedance) is given by:

$$I_S = (1 - \rho_T) \sum_{i=1}^{\infty} (R_i^P + R_i^N) , \tag{35}$$

or:

$$I_S = \frac{I_0}{2} \left[(\Gamma_1 + \Gamma_2 - \rho_1 - \rho_2) + (\Gamma_1 - \Gamma_2 - \rho_1 + \rho_2) \left(\frac{\Lambda_0}{1 - \Lambda_1} \right) \right] . \tag{36}$$

The expressions for the total current driven into the load impedance, into the ferrite-loaded transmission line, and reflected back down the drive cable to the source have been derived for the DCB-1. All reflections and multiple reflections have been included. These expressions will later be used to give the current and power delivered into the Ellipticus antenna.

II. BALANTENNA EQUIVALENT CIRCUIT

The Balantenna **[6]** was designed as a balun structure which mitigates the high-frequency ringing associated with the use of dual coaxial cables. The 100 ohm cables have been shortened to zero length and the output of the 50 ohm cable drives a pair of 100 ohm transmission lines which are on the exterior of the Balantenna structure, and which transition gradually to the impedance of the cables which form the Ellipticus antenna **[4]**.

The first version of the Balantenna, **Figure 6**, has the equivalent circuit shown in **Figure 7**. There are not any 100 ohm coaxial cables in this balun, so no multiple reflections occur within the cables. The two 100 ohm sections are the input to the transmission lines on each side of the drive point. The ferrite-loaded back impedance is located directly in parallel with the two halves of the output antenna impedance, directly across the output of the 50 ohm coax. It is contained within the conducting metal sheets which form the disc or "hub" of the Balantenna.

The load impedance seen by the drive cable is the parallel impedances of the two halves of the antenna and the back impedance:

$$Z_L = \left(\frac{1}{Z_B} + \frac{2}{Z_A} + \frac{2}{Z_A} \right)^{-1} = \frac{Z_A Z_C}{Z_A + 4Z_B} . \tag{37}$$

The reflection coefficient is given by:

$$\rho = \frac{Z_A Z_B - Z_A Z_C - 4 Z_B Z_C}{Z_A Z_B + Z_A Z_C + 4 Z_B Z_C} . \tag{38}$$

The current into the load impedance is:

$$I_L = I_0 (1 - \rho) . \tag{39}$$

The current into the antenna is then:

$$I_A = I_L \left(\frac{Z_B}{Z_L} \right) , \tag{40}$$

and the current into the ferrite is:

$$I_B = I_L \left(\frac{Z_A}{4 Z_L} \right) . \tag{41}$$

The current reflected back down the drive cable is:

$$I_R = -\rho I_0 . \tag{42}$$

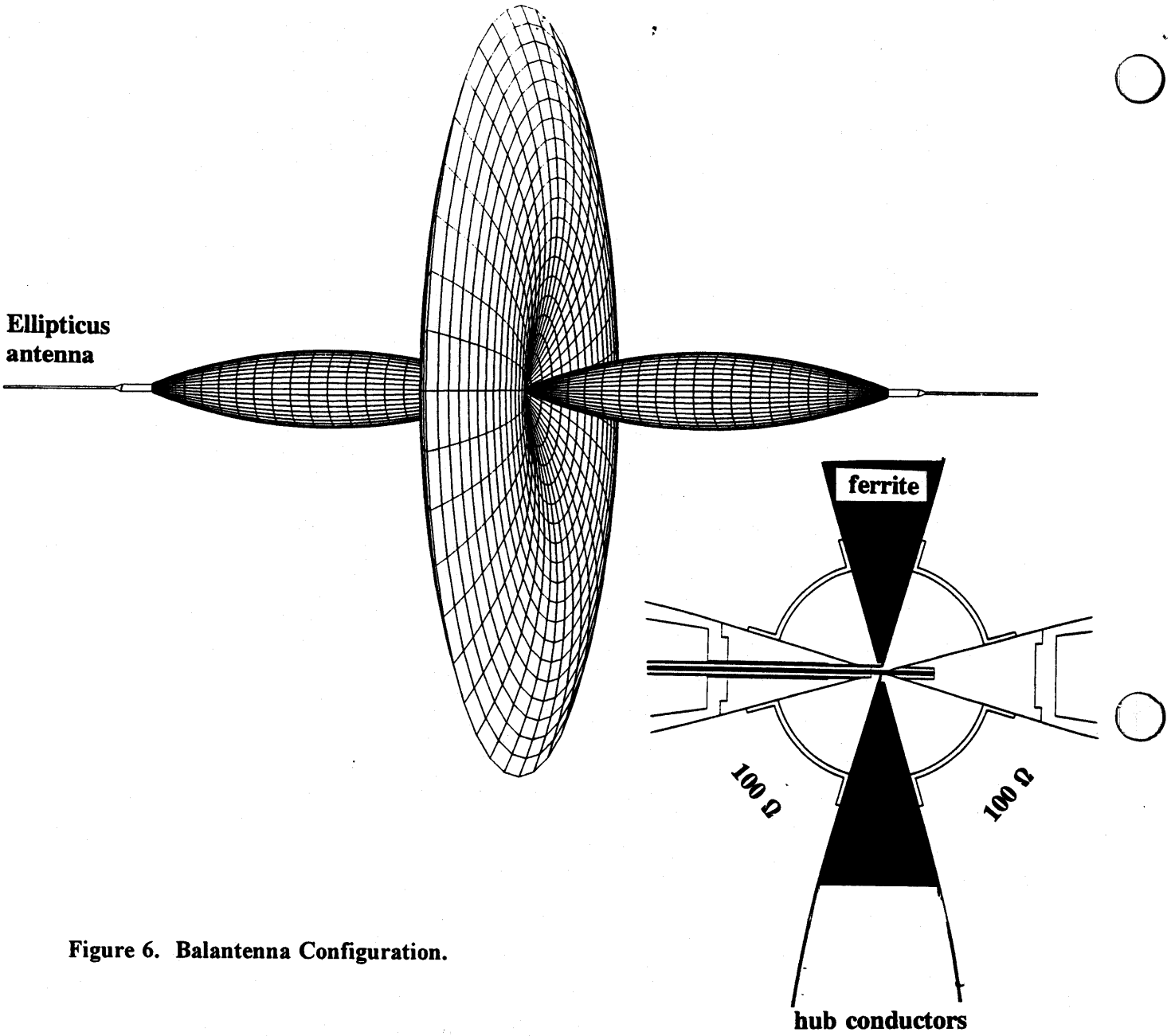

Figure 6. Balantenna Configuration.

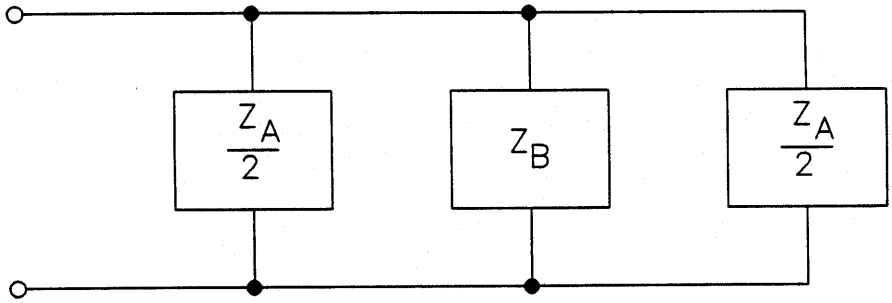

Figure 7. Balantenna Equivalent Circuit.

III. TRANSMISSION LINE IMPEDANCE

The ferrite-loaded back impedance is a transmission line, terminated in a short circuit. The impedance of this transmission line, without its ferrite loading, should be of constant value, at least in a linear piece-wise fashion, as given by the distributed inductance and capacitance of the line:

$$Z_0 = \sqrt{\frac{j\omega L_0}{j\omega C_0}} . \tag{43}$$

For the coaxial line this is:

$$Z_0 = \frac{\eta}{2\pi} \ell n\left(\frac{b}{a}\right), \tag{44}$$

with b the diameter of the housing and a the diameter of the coax jacket. η is the free-space wave impedance:

$$\eta = \sqrt{\frac{\mu_0}{\epsilon_0}} = \mu_0 c , \tag{45}$$

where c is the speed of light.

The impedance of the biconical transmission line of the balantenna is given by:

$$Z_0 = \frac{\eta}{\pi} \ell n\left[\cot\left(\frac{\theta_0}{2}\right)\right], \tag{46}$$

where θ_0 is the half-angle of the cone.

When the transmission line is terminated in its characteristic impedance, there is no reflection from the far end of the line (at the load), and the input impedance to the line is identically equal to the characteristic impedance. When it is terminated in a generalized load impedance Z_L, the input impedance is:

$$Z(IN)_1 = Z_0 \frac{Z_0 + Z_L \tanh(\gamma d)}{Z_L + Z_0 \tanh(\gamma d)} . \tag{47}$$

where γ is the propagation constant and d is the length of the line. If another transmission line, of a different characteristic impedance, is connected to the input of the first line, then its load impedance is that given by the above expression. The input impedance of this new section is then given by an the same formulation, with the impedance parameters modified as:

$$Z(IN)_2 = Z_2 \frac{Z_2 + Z(IN)_1 \tanh(\gamma_2 d_2)}{Z(IN)_1 + Z_2 \tanh(\gamma_2 d_2)} . \tag{48}$$

This cascading process can be continued indefinitely.

The DCB-1 is constructed with two discreet sections of ferrite loading: 21.6 cm of nickel-zinc (Ni-Zn) ferrite followed by 43.2 cm of manganese-zinc (Mn-Zn) ferrite. The Ni-Zn ferrite acts as a high-frequency impedance, and is the first impedance seen by the back currents. The Mn-Zn ferrite is a low-frequency impedance. The above equations are used to obtain the back impedance for this configuration.

The Balantenna is constructed with a single section of Ni-Zn ferrite, 10 cm in radius. Future calculations and models may incorporate ferrite powder (perhaps in a dielectric matrix) exterior to the solid section in order to provide extra impedance.

IV. FERRITE INTRINSIC (WAVE) IMPEDANCE

The frequency-dependant intrinsic properties of any material are given in terms of the complex permittivity:

$$\epsilon^{\star}(\omega) = \epsilon_0[\epsilon'(\omega) - j\epsilon''(\omega)] , \tag{49}$$

and the complex permeability:

$$\mu^{\star}(\omega) = \mu_0[\mu'(\omega) - j\mu''(\omega)] , \tag{50}$$

where the asterisk denotes the complex quantity, and all of the primed quantities are the dimension-less ratios. The imaginary parts represent the losses within the material, including those due to the conductivity. The dielectric loss mechanism described applies to a material which has only bound charges. For a material with appreciable charge carriers there exists an ordinary conductivity which relates the current density to the applied field:

$$I = \sigma E . \tag{51}$$

At any given frequency, this loss and that described for the bound charges add directly, so it is common to include it in the ϵ'' term, or to define an equivalent conductance which describes all losses:

$$\sigma = \omega \epsilon'' . \tag{52}$$

The complex intrinsic impedance in the material is given by:

$$Z_f(\omega) = \sqrt{\frac{\mu^{\star}(\omega)}{\epsilon^{\star}(\omega)}} = \eta \sqrt{\frac{\mu'(\omega) - j\mu''(\omega)}{\epsilon'(\omega) - j\epsilon''(\omega)}} , \tag{53}$$

and the complex propagation constant by:

$$\gamma(\omega) = j\omega\sqrt{\mu^{\star}(\omega)\epsilon^{\star}(\omega)} = \gamma_0 \sqrt{[\mu'(\omega) - j\mu''(\omega)]\,[\epsilon'(\omega) - j\epsilon''(\omega)]} . \tag{54}$$

The propagation constant in vacuum is given in terms of the free-space properties:

$$\gamma_0 = j\omega\sqrt{\mu_0 \epsilon_0} = \frac{j\omega}{c} . \tag{55}$$

If the complex permittivity and permeability are known, then the complex intrinsic impedance and propagation constant can be accurately calculated. Unfortunately, these properties are not well characterized for ferrites, especially over the frequency ranges of interest for high-frequency, high-power baluns. The permeability and loss properties of magnetic materials are usually furnished by the manufacturers, but not for very high frequencies. The highest frequency for which we have seen data is 1000 MHz, recently extended from 100 MHz, but 100 kHz is more typical.

Approximate analytical models of the ferrite can be constructed using the **Debye equations [7], [8]**:

$$\epsilon^{\star}(\omega) \approx \epsilon_{\infty} + \frac{\epsilon_s - \epsilon_{\infty}}{1 + j\omega\tau_{\epsilon}} = \epsilon_{\infty} + \frac{(\epsilon_S - \epsilon_{\infty})(\omega_{\epsilon}^2 - j\omega_{\epsilon}\omega)}{\omega_{\epsilon}^2 + \omega^2}, \tag{56}$$

$$\mu^{\star}(\omega) \approx \frac{\mu_0}{1 + j\omega\tau_{\mu}} = \mu_0 \frac{\omega_{\mu}^2 - j\omega_{\mu}\omega}{\omega_{\mu}^2 + \omega^2}. \tag{57}$$

where ϵ_s is the static permittivity (approaching zero frequency), ϵ_∞ is the high frequency permittivity, and τ_ϵ is the dielectric relaxation time constant. $\tau_\epsilon = 1/\omega_\epsilon$ describes a material with a single dielectric relaxation time, and $\tau_\mu = 1/\omega_\mu$ describes a material with a single magnetic relaxation time; the two are unrelated because they are due to totally unrelated physical processes.

Typical ferrites seem to exhibit a mxture of two or more magnetic relaxation times, perhaps because they are indeed mixtures of different materials or different phases of the same material.

<u>Manganese-Zinc Ferrite:</u> These equations are plotted in **Figures 8** and **9** for a hypothetical Mn-Zn ferrite with the parameters shown. This is a low-frequency ferrite with high conductivity and a resulting large imaginary permittivity. For a homogeneous mixture of different ferrites with different static properties and relaxation times, the properties of each part add proportionally to give the properties of the whole.

With the model given by the Debye equations above, the wave impedance and attenuation within the ferrite can be calculated, as seen in **Figures 10** and **11**. The propagation Ψ into the material may be defined as:

$$\Psi = e^{-\gamma d}, \tag{58}$$

where d is the depth of propagation. Only the real part of the attenuation is shown as:

$$\left|e^{-\gamma \ell}\right| = e^{-\alpha \ell}, \tag{59}$$

where α is the real part of γ, and multiples of a unit length of one centimeter are plotted.

<u>Nickel-Zinc Ferrite:</u> The Debye equations for a typical Ni-Zn ferrite are plotted in **Figures 12** and **13**. This high-frequency ferrite has a very high resistivity (10^9 ohm-cm) which results in a near zero value for the imaginary permittivity. The value given for the real part of the permittivity ranges from 10 to 20; the value of 16 is arbitrarily used here. **Figures 14** and **15** show the wave impedance and attenuation within this ferrite.

V. IMPEDANCE WITH FERRITE IN TRANSMISSION LINE

The characteristic impedance of the transmission line with the ferrite is given by:

$$Z_C = \sqrt{\frac{R + j\omega L}{G + j\omega C}}, \tag{60}$$

where R and L are the series resistance and inductance per unit length, and G and C are the shunt conductance and capacitance per unit length.

The series impedance per unit length then becomes:

$$R + j\omega L = j\omega L_0 [\mu' - j\mu''] = j\omega L_0 \mu^{\star}(\omega) , \tag{61}$$

and the shunt admittance per unit length:

$$G + j\omega C = j\omega C_0 [\epsilon' - j\epsilon''] = j\omega C_0 \epsilon^{\star}(\omega) . \tag{62}$$

The wave impedance then becomes:

$$Z_C = \sqrt{\frac{j\omega L_0 \mu^{\star}(\omega)}{j\omega C_0 \epsilon^{\star}(\omega)}} = \frac{Z_0 Z_I}{\eta}, \tag{63}$$

The propagation constant is given by:

$$\gamma = \sqrt{[R + j\omega L]\,[G + j\omega C]} = \gamma_0 \sqrt{\mu^{\star}(\omega)\epsilon^{\star}(\omega)} . \tag{64}$$

where

$$\gamma_0 = j\omega\sqrt{L_0 C_0} = \frac{j\omega}{c} \tag{65}$$

is the propagation constant of the empty fixture.

The results of this section are very significant:

The characteristic impedance is directly proportional to the impedance of the empty transmission line times the wave impedance of the ferrite. Both of these need to be made large in order to obtain a large back impedance to the unwnated currents.

The propagation coefficient is just that of the ferrite and is independent of the transmission line geometry.

VI. COAXIAL FERRITE BEADS IN TRANSMISSION LINES

When homogeneous mixtures of different materials are used, the permeabilities and the inverses of the permittivities are proportionally additive to give the bulk properties:

$$\mu^{\star}(\omega) = \sum_i a_i \, \mu_i^{\star}(\omega) \, , \qquad \frac{1}{\epsilon^{\star}(\omega)} = \sum_i \frac{a_i}{\epsilon_i^{\star}(\omega)} \, , \tag{66}$$

where the a_i are the proportionality coefficients. For beads of different ferrites coaxially placed over each other within the transmission line, these equations approximately apply (in actuality, the wave equations must be solved within each ferrite and the boundary conditions at the interfaces matched). When the ferrite properties are measured as in **Section VIII**, the measurements automatically give the correct results. The DCB-1 is constructed with two nested sets of ferrite beads which both have outside diameter/inside diameter ratios of two, so the value of ½ is used for the a_i .

VII. CASCADED TRANSMISSION LINES

The ferrite transmission line within the balun is terminated at its far end in a short circuit.The low-frequency ferrite material model of the above figures then gives the input impedance of this terminal section shown in **Figure 18**. The resonances of this line occur at very low frequencies because the velocity of propogation is very slow, a result of the large permeability and permittivity at low frequency.

A high-frequency, high resistivity ferrite material is then used for the input section to the transmission line, which has the wave impedance of **Figure 10**. The high resistivity results in a purely real permittivity (over the entire frequency range of interest), equal to the DC value.

The characteristic impedance of this material in the transmission line is shown in **Figure 16**. The resulting input impedance to this cascaded transmission line is shown in **Figure 19.** The resonance at 3 MHz is due to the electrical length of the Ni-Zn ferrite.

VIII. TECHNIQUES TO MEASURE FERRITE PROPERTIES

The above analysis is based on *a priori* knowledge of the ferrite complex permittivity and permeability. These quantities are usually not known for the particular ferrite materials of interest. For the analysis to be subsequently presented, the required properties are the wave impedance and propagation constant. If either pair of these complex quantities are known, the other pair is readily obtained from equations **(63)** and **(64)**.

Transmission line fixtures can be used to determine these properties **[9]**. When the ferrite section of impedance $Z_B(\omega)$ is driven from in input characteristic impedance Z_0 and terminated in an impedance Z_1, the total reflection coefficient is:

$$S_{11} = \frac{\rho_1 + \rho_2 e^{-2\gamma d}}{1 + \rho_1 \rho_2 e^{-2\gamma d}} = \frac{\rho_1 + \rho_2 \Psi^2}{1 + \rho_1 \rho_2 \Psi^2} , \tag{67}$$

where S_{11} is also the input scattering parameter as measured with an S-parameter test set on a network analyzer. The reflection coefficient into the ferrite is:

$$\rho_1 = \frac{Z_B - Z_0}{Z_B + Z_0} , \tag{68}$$

and that out of the ferrite into the load impedance is:

$$\rho_2 = \frac{Z_1 - Z_B}{Z_1 + Z_B} . \tag{69}$$

Inserting these two reflection coefficients into the expression for the total reflection gives:

$$S_{11} = \frac{Z_{IN} - Z_0}{Z_{IN} + Z_0} . \tag{70}$$

which is the total reflection coefficient given by the usual impedance relation. This can then be solved for the input impedance to the ferrite-loaded transmission line:

$$Z_{IN} = Z_0 \frac{1 + S_{11}}{1 - S_{11}} . \tag{71}$$

Reflections with opens and shorts at end of ferrite: When the output of the ferrite is directly terminated in a short circuit, the load reflection coefficient ρ_2 is **-1**, and the input impedance reduces to:

$$Z_{SC} = Z_B(\omega) \tanh(\gamma d) . \tag{72}$$

When it is terminated in an open it becomes:

$$Z_{OC} = Z_B(\omega) \coth(\gamma d) . \tag{73}$$

Data sets can be taken in these two configurations and processed to give the open-circuit and short-circuit input impedances (some network analyzers do this internally as a menu function), and then solved for the characteristic impedance and propagation constant:

$$Z_B(\omega) = \sqrt{Z_{O.C.} \times Z_{S.C.}} \tag{74}$$

$$\gamma(\omega) = \frac{1}{d} \, Arctanh \sqrt{\frac{Z_{S.C.}}{Z_{O.C.}}} \, . \tag{75}$$

Because of the large variation over frequency of the intrinsic ferrite properties, measurements may be required for different lengths of ferrite-loaded transmission line in order to obtain adequate signal strengths for data processing and display. This is particularly true for the determination of the propagation constant because of the division process.

Ferrite Section in Coaxial Line: Another configuration that can be used to obtain the ferrite parameters of interest is that of a transmission line filled with a ferrite material for a length ***d***, **[10]**. Most ferrite beads are not of a dimension that fit within and fill a 50 ohm air transmission line (unless they are specially machined), so the empty impedance of this section may be made to be different than that of the reference lines (50 ohms) on each side. Care must be used in making the transitions in the geometry at these points so that reflections from the resulting impedance discontinuities are minimized.

The total transmission coefficient (ratio of output voltage signal-to-input voltage signal) is given by:

$$S_{21} = \frac{(1 - \rho_1)(1 - \rho_2)\Psi}{1 + \rho_1 \rho_2 \Psi^2} \, . \tag{76}$$

The input reflection coefficient is the same as the general expression obtained above, except that the load impedance is now that of the empty transmission line of impedance Z_0, and the reflection coefficient at the output of the ferrite is:

$$\rho_2 = -\rho_1 \, . \tag{77}$$

The input reflection coefficient is then:

$$S_{11} \equiv \frac{\rho_1(1 - \Psi^2)}{1 - \rho_1^2 \Psi^2} \, . \tag{78}$$

The transmission coefficient reduces to:

$$S_{21} = \frac{\left(1 - \rho_1^2\right)\Psi}{1 - \rho_1^2 \Psi^2} . \tag{79}$$

Note that these two S-parameters do not add to unity, because of the losses in the ferrite.

These results allow for the calculation of the coefficients ρ_1, Ψ, S_{11}, and S_{21} for a line with a material of known $\epsilon^\star$ and $\mu^\star$. The parameters which can be measured are S_{11} and S_{21}, so the above equations must be solved for ρ_1 and Ψ, giving:

$$\rho_1 = \lambda + \sqrt{\lambda^2 - 1} , \tag{80}$$

$$\Psi = \frac{S_{11} + S_{21} - \rho_1}{1 - \left(S_{11} + S_{21}\right)\rho_1^2} , \tag{81}$$

with

$$\lambda = \frac{S_{11}^2 - S_{21}^2 + 1}{2 S_{11}} . \tag{82}$$

Note that nulls in the measured values of S_{11} will result in discontinuities in these parameters. Great care must be exercised in the data acquisition and/or filtering or smoothing techniques employed to prevent such nulls.

The intrinsic parameters are then:

$$\gamma(\omega) = -\frac{\ell n(\Psi)}{d} = j\omega\sqrt{\mu^\star(\omega)\epsilon^\star(\omega)} , \tag{83}$$

$$Z_B(\omega) = Z_0 \frac{1 + \rho_1}{1 - \rho_1} = \frac{Z_0}{\eta} Z_I(\omega) = \frac{Z_0}{\eta} \sqrt{\frac{\mu^\star(\omega)}{\epsilon^\star(\omega)}} . \tag{84}$$

This results in the complex permittivity and permeability as:

$$\epsilon^\star(\omega) = \frac{\gamma(\omega)}{j\omega Z_I(\omega)} , \tag{85}$$

$$\mu^{\star}(\omega) = \frac{\gamma(\omega)\, Z_I(\omega)}{j\,\omega} \,. \qquad (86)$$

For measurements resulting in accurate determination of the intrinsic parameters, the ferrite must exactly fill the test fixture section of the transmission line, with all voids filled with liquid metal or some other technique. For the case of interest here, the determination of the properties of practical transmission lines with commercially available ferrite beads and air gaps in the lines, the measurements that give Z_B and γ under these conditions is preferable.

Two alternate techniques are formulated for measuring the characteristic impedance and propagation constant of a ferrite-loaded transmission line. These two measurement sets can be acquired using the same measurement instrumentation and only slight differences in test fixtures. The results of the measurements and analysis can then be directly compared.

IX. ANTENNA IMPEDANCE

The impedance of the ferrite-loaded transmission line in combination with the antenna impedance give the total load impedance at the balun output, **Figure 2**. The antenna impedance must be accurately known for subsequent signal analysis.

Previous Data: **Figure 20** shows the measured impedance of the earlier Ellipticus antenna [5]. This is not the impedance of the present antenna with the smaller cable diameter and resistively-loaded ferrite chokes [7]. It is, however, the only measurement presently available and so is used here with the knowledge that it is of limited accuracy.

The load impedance for the positive coaxial cable, **Figure 3** and equation **(1)** is shown in **Figure 22**. It is dominated by the large impedance of the antenna. The reflection coefficient, equation **(2)**, is **Figure 23**.

The results for the negative cable, **Figure 4** and equations **(3)** and **(4)** are shown in **Figures 24** and **25**. These are dominated by the back impedance rather than the antenna impedance.

Analytical Antenna Model: An analytical model for the ELLIPTICUS antenna with the ferrite/resistive loading described in [7] is also used. **Figure 21** shows the real and imaginary components of this impedance. It is significantly different than that of **Figure 20**: The resonances at and below one Megahertz from the antenna dimensions are not included, and the magnitudes of the components are larger at the frequency extremes. The imaginary part is mostly positive instead of negative, except at the highest frequencies where it is modelled as a capacitive element due to the geometry of the connection to the positive antenna wire (dummy cable).

> **The actual antenna impedance probable resembles neither of these figures. Only actual measurements will give the true value. At high frequencies, the antenna impedance for the Balantenna will differ significantly from that for the DCB-1 attached to the Ellipticus antenna because of the differences in the balun geometries. Both of these systems need to be characterized with the antenna.**

X. POWER LEVELS

The power dissipated in any impedance by the current flowing through it is the square of the magnitude of that current (or the magnitude of the square of the current) times the real part of the impedance as given by equation **(36)**.The power delivered by any of these total currents into their load is the square of the magnitude of that current times the real part of the load impedance:

$$P = |I^2| \ \Re e\{Z\} \ . \qquad (87)$$

The current into the antenna from the DCB-1 is given by equation **(32)**, and is shown in **Figure 26**. The antenna impedance used here is that for the previous Ellipticus antenna measurement, **Figure 22**.The current rises to the source current value (two Amperes) at low frequencies because the antenna impedance becomes very nearly zero at these frequencies.

The current into the ferrite is that of equation **(33)**, and that lost back down the source cable is equation **(35)**. The respective powers into these three impedances, assuming a source power of 200 Watts, are shown in **Figure 27**. The three power levels add to give the incident power at all frequencies. The antenna impedance used here is that for the previous Ellipticus antenna measurement.

The power is attenuated as it propagates into the ferrite, equation **(58)**. The power levels remaining at one-centimeter increments into the ferrite are shown in **Figure 28**. It is observed that most of the power is dissipated within the first centimeter.

XI. THERMAL ASPECTS

The power attenuated by the ferrite results in energy being deposited in it. For each incremental section of ferrite, this is the input power minus the output power, times the duration of time that the power is deposited. A one-hundred second sweep across the frequency band of **Figure 28** (typical for Ellipticus) gives the energy distribution into the ferrite shown in **Figure 29.**

This energy results in a temperature increase of the ferrite. The specific energy of the ferrite is about 5.0 cal/gm and the density about 3.0 gm/cm^3. The temperature rise per sweep is shown in **Figure 30.** The Curie temperature of the ferrite is about 125-130 degrees Centigrade, which can be exceeded in just a few sweeps for the model balun just described (that of the first prototype unit used in Ellipticus). The temperature rise at the surface of the first ferrite bead is printed on **Figure 27** , the plot of the power levels.

XII. OTHER RESULTS

Analytical model of the ferrite-loaded new Ellipticus antenna: The antenna current and power levels for the analytical model of the ferrite-loaded new Ellipticus antenna (**Figure 21**) are in **Figures 31** and **32**. This model gives much broader and flatter drive into the antenna, particularly at the lower frequencies. The performance at the higher frequencies is somewhat diminished due to the higher antenna impedance values.

Prototype DCB: A prototype DCB had been previously constructed which exhibited erratic performance and failures which were traceable to excessive temperatures. Temperature markers placed on the ferrite beads showed that the first beads did indeed exceed their Curie temperature. The power levels for this balun are shown in **Figure 33**, with the calculated temperature rise indicating that excessive heating indeed occurred, the Curie temperature being reached in just a few sweeps.

This prototype had a lower characteristic ferrite impedance, as well as a smaller ferrite mass per unit length by a factor of five, than does the DCB-1. The insulating fiberglass housing of the prototype unit was eliminated from the DCB-1, leaving the bare aluminum balun housing exposed to the ambient air, underneath a sun shield, for better cooling.

Balantenna: The analytical results for the first model of the **Balantenna** yield results that are not encouraging! **Figure 34** shows the projected power into the antenna, which is much lower than that from the DCB-1, **Figure 27**. Significantly more power is absorbed by the ferrite than goes onto the antenna. This inferior performance can be attributed to the low transmission line back impedance of 17.6 ohms compared to the 83 ohms of the DCB-1.

The temperature rise of the front face of the ferrite of this balantenna is more than one hundred times that of the DCB-1, more than enough to exceed the Curie temperature in a single sweep. This is because of the small frontal area of this balantenna design, 4.2 square millimeters *vs* 475 square millimeters for the DCB-1.

One obvious way in which to improve the performance of the Balantenna is to make the incident face of the ferrite much larger, which increases the impedance of the transmission line and reduces the current that flows into the ferrite, and increases the volume of ferrite into which the energy is dissipated.

200 Ohm Load on DCB-1: **Figure 35** shows the power driven into a 200 ohm resistive load. Such a load, constructed from low-inductance resistors with 50 of the ohms being a coaxial cable into the measurement port of an analyzer, is useful for characterizing the balun. The results shown here are very similar to measurements performed in Reference **[5]**.

XIII. CONCLUSIONS and RECOMMENDATIONS

The results presented in this paper are based upon theoretical models for the ferrite used within the baluns and for the impedance of the Ellipticus antenna. These results tend to agree with the limited data available. They also generally agree with the field-mapping results in the Ellipticus simulator with the new ferrite-loaded antenna and the DCB-1 driver. The models used for the analytical ferrite properties thus seem to be reasonably accurate.

These results allow for the parametric design of a balun by the variance of ferrite types and sizes, therefore predicting the performance of a balun before it is constructed. Comparison of alternate balun designs can be performed, and relative behavior studied.

The models used within this paper need to be replaced with actual data. **Section VI** details a method with which the complex impedance of the ferrite loading of the DCB-1 and Balantenna can be measured, so that **Figure 8** and all subsequent figures can be replaced with calculations based on actual ferrite properties. Actual ferrite geometries in transmission lines can then be analyzed, specific to particular balun designs.

The impedance of the antenna can be measured in the time domain with a high voltage TDR system to over-ride the radio frequency noise induced onto the antenna by local radio stations. A Fourier transform of the TDR waveform will then give the actual complex frequency domain impedance of the antenna, so that **Figure 20** and all subsequent figures can be replaced.

The ferrite and antenna measurements need to be performed so that accurate analysis can be performed before the balantenna is re-designed and constructed.

The Balantenna can then be designed and constructed with acceptable performance, with significant power delivered to the Ellipticus antenna, low power and heat dissipated in the ferrite, and without the high-frequency cable resonances as in the DCB-1.

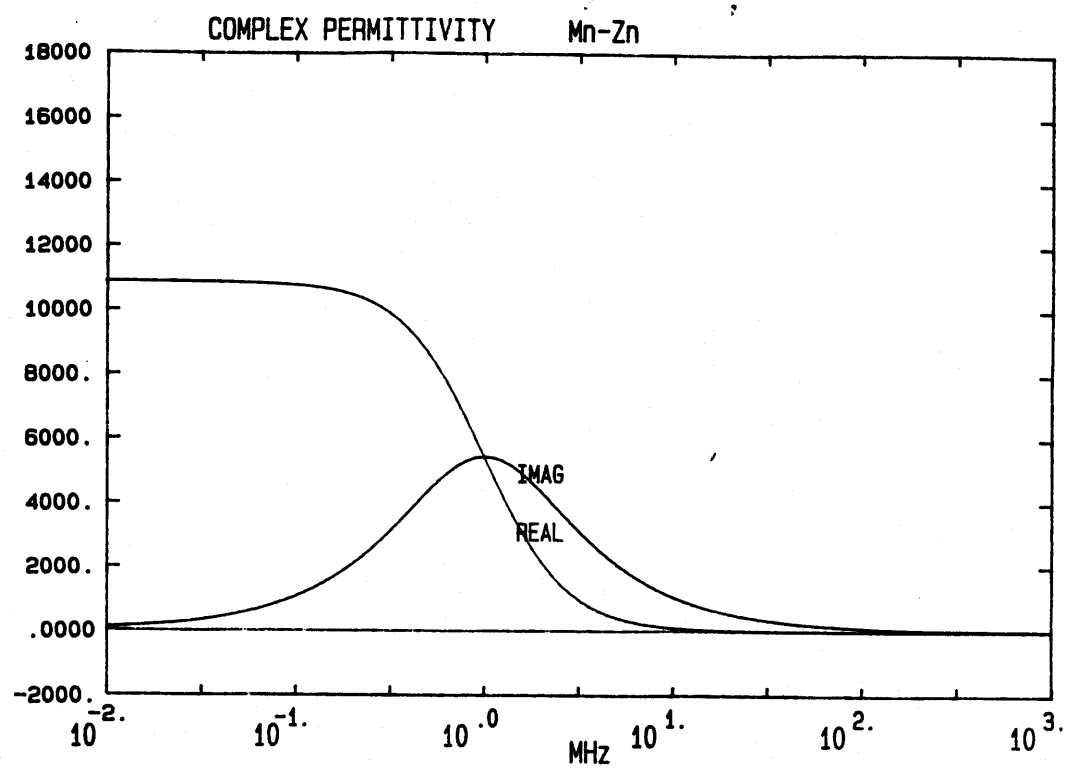

Figure 8. Complex Permittivity Model of Mn-Zn Ferrite.

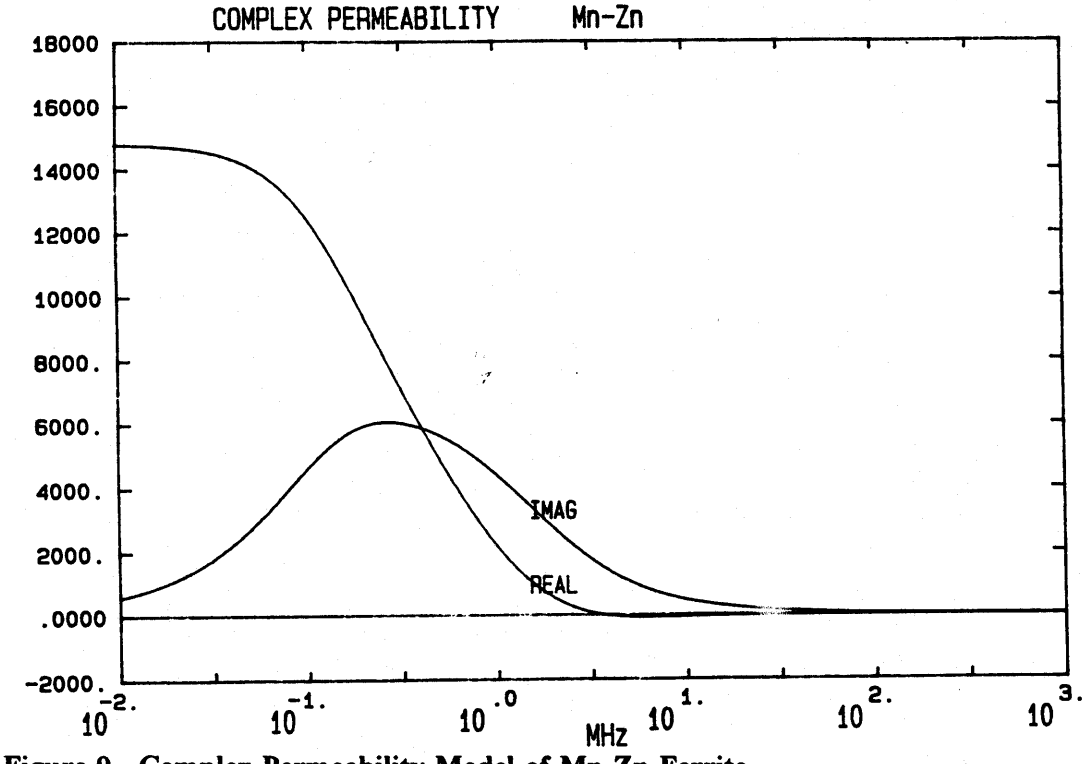

Figure 9. Complex Permeability Model of Mn-Zn Ferrite.

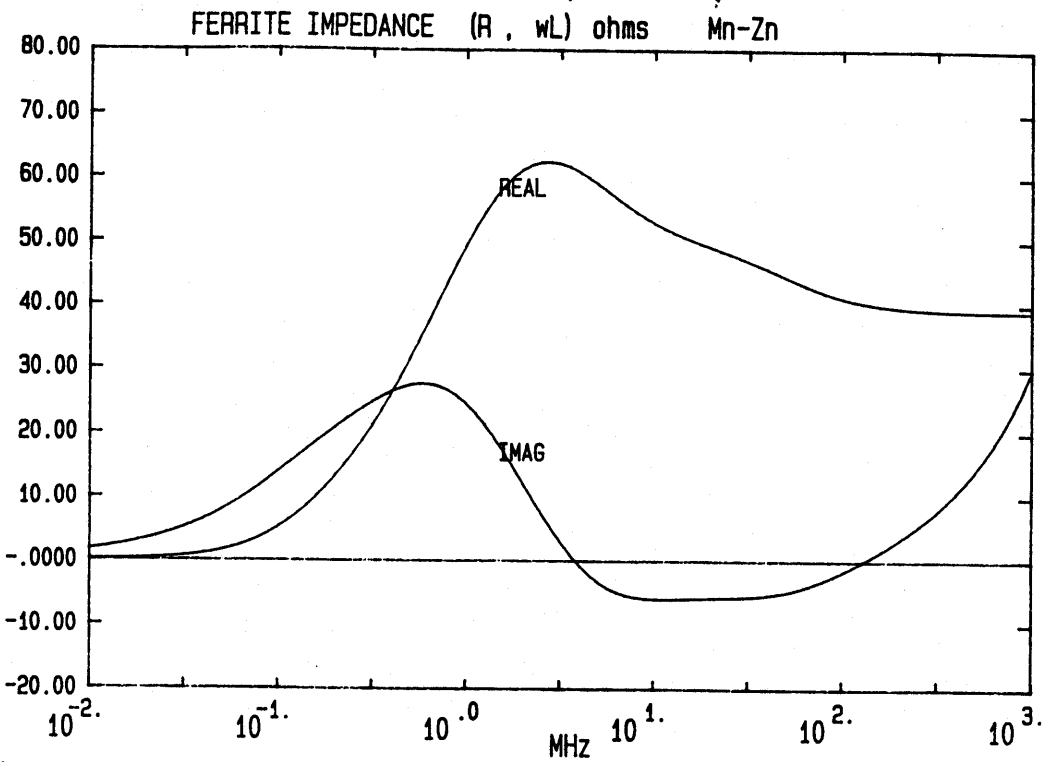

Figure 10. Complex Wave Impedance of Mn-Zn Ferrite.

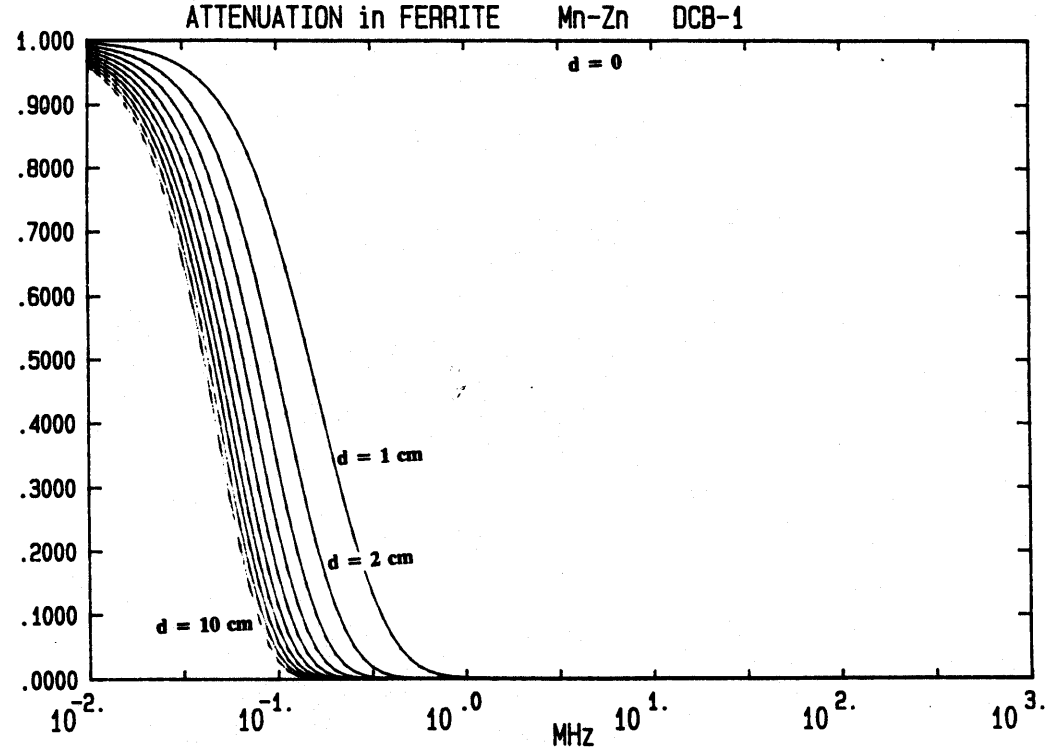

Figure 11. Attenuation Within Mn-Zn Ferrite.

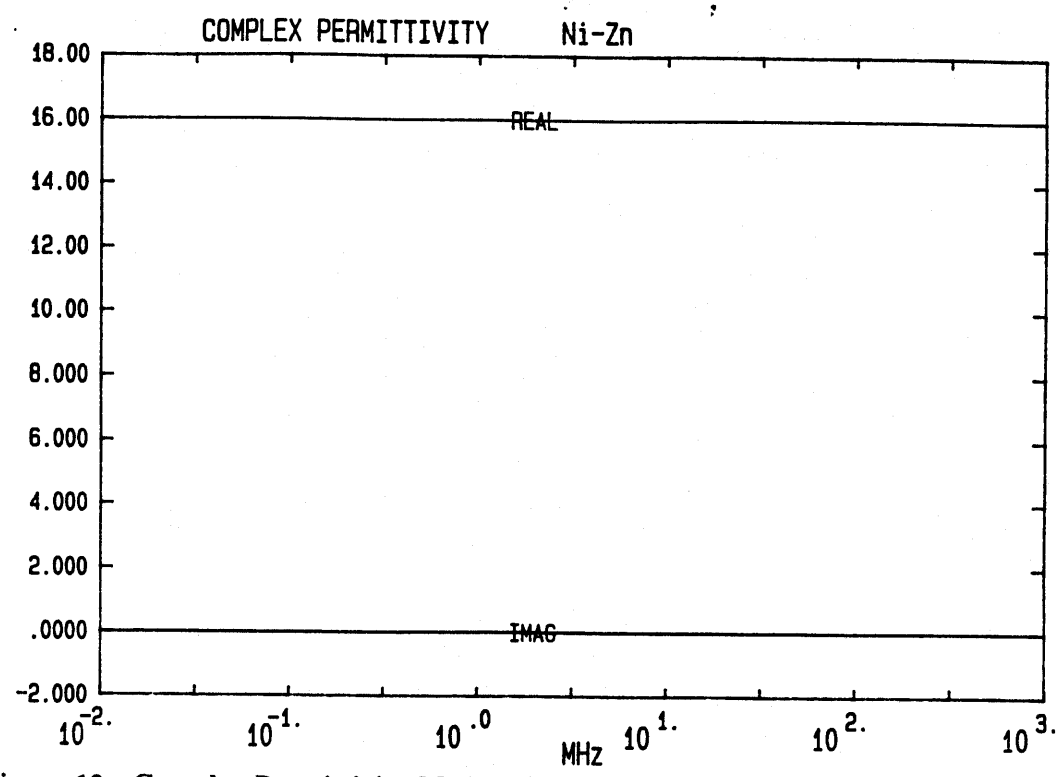

Figure 12. Complex Permittivity Model of Ni-Zn Ferrite.

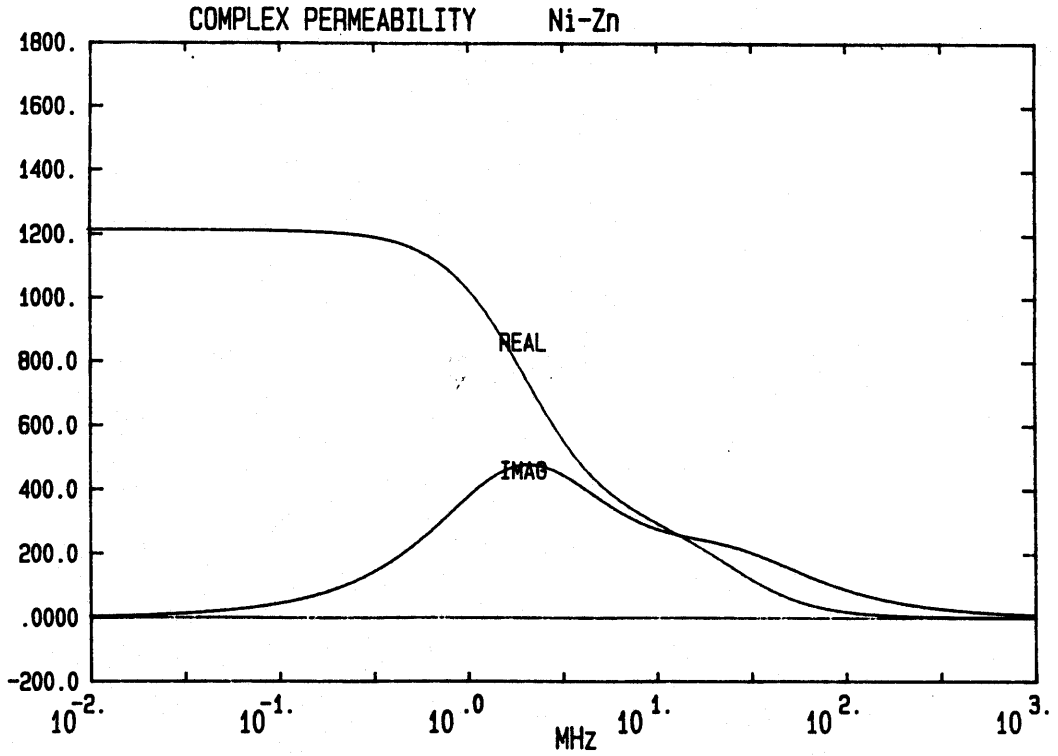

Figure 13. Complex Permeability Model of Ni-Zn Ferrite.

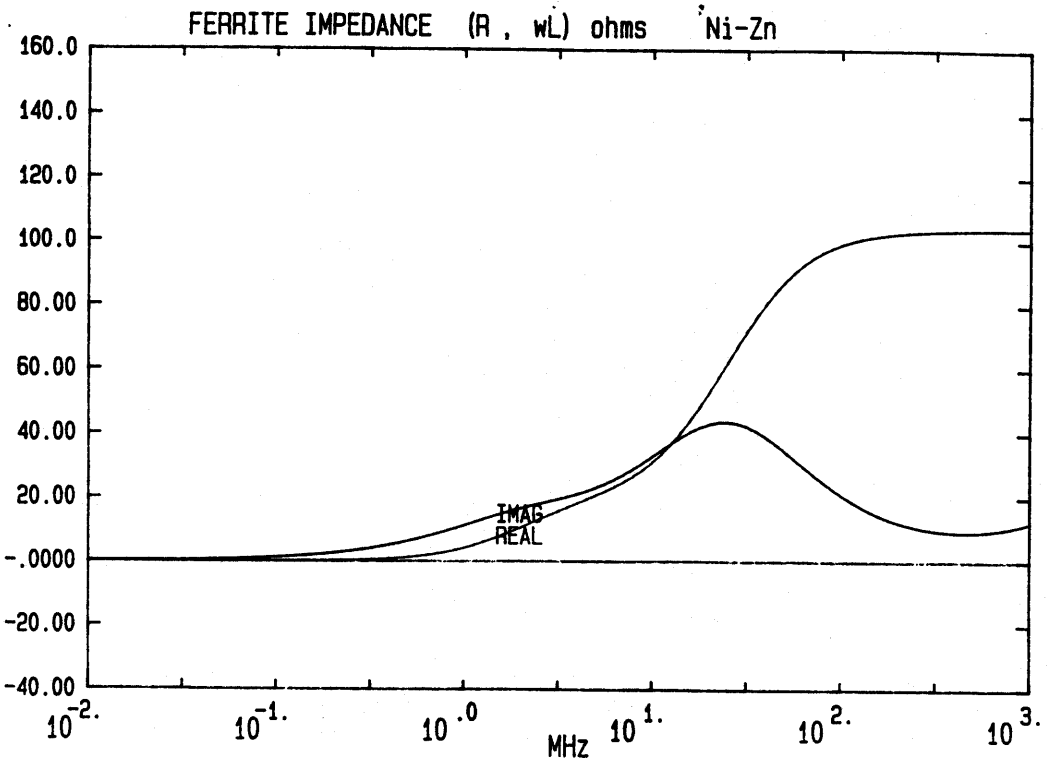

Figure 14. Complex Wave Impedance of Ni-Zn Ferrite.

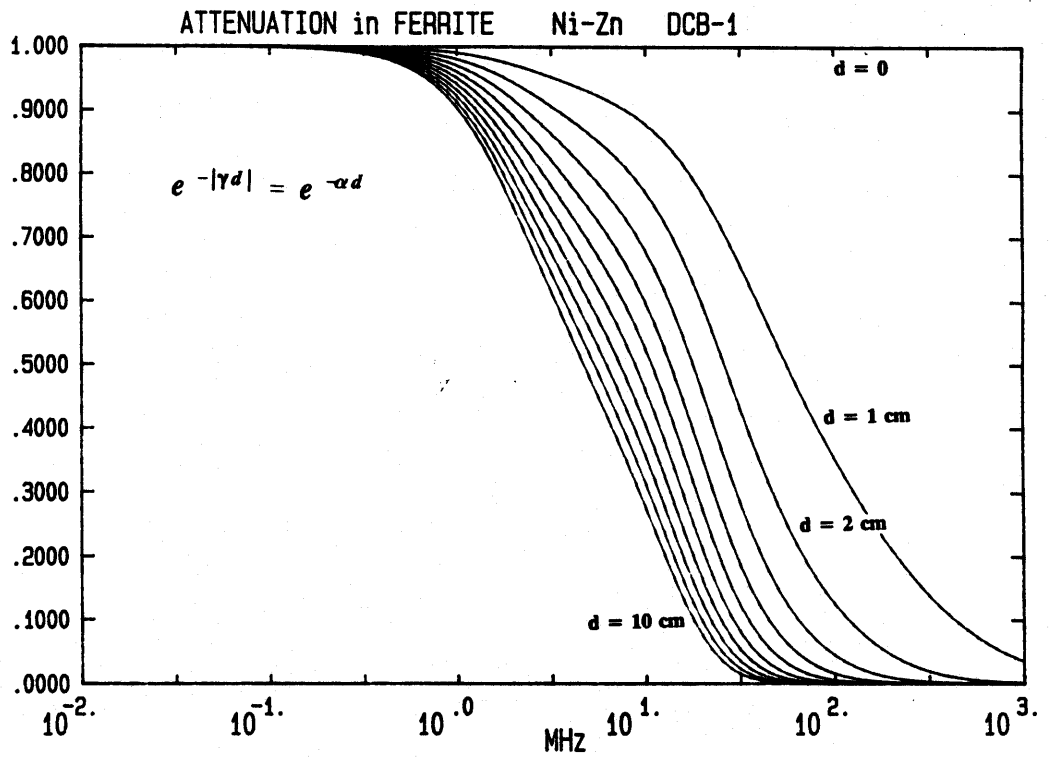

Figure 15. Attenuation Within Ni-Zn Ferrite.

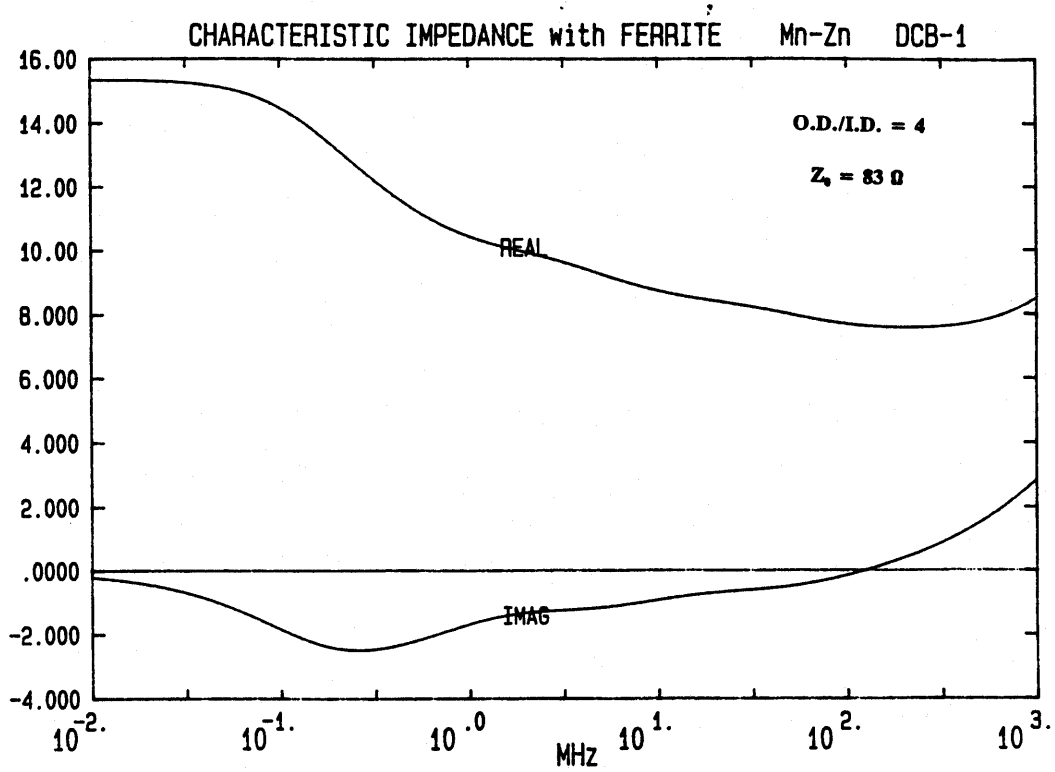

Figure 16. Characteristic Impedance of Line with Mn-Zn Ferrite.

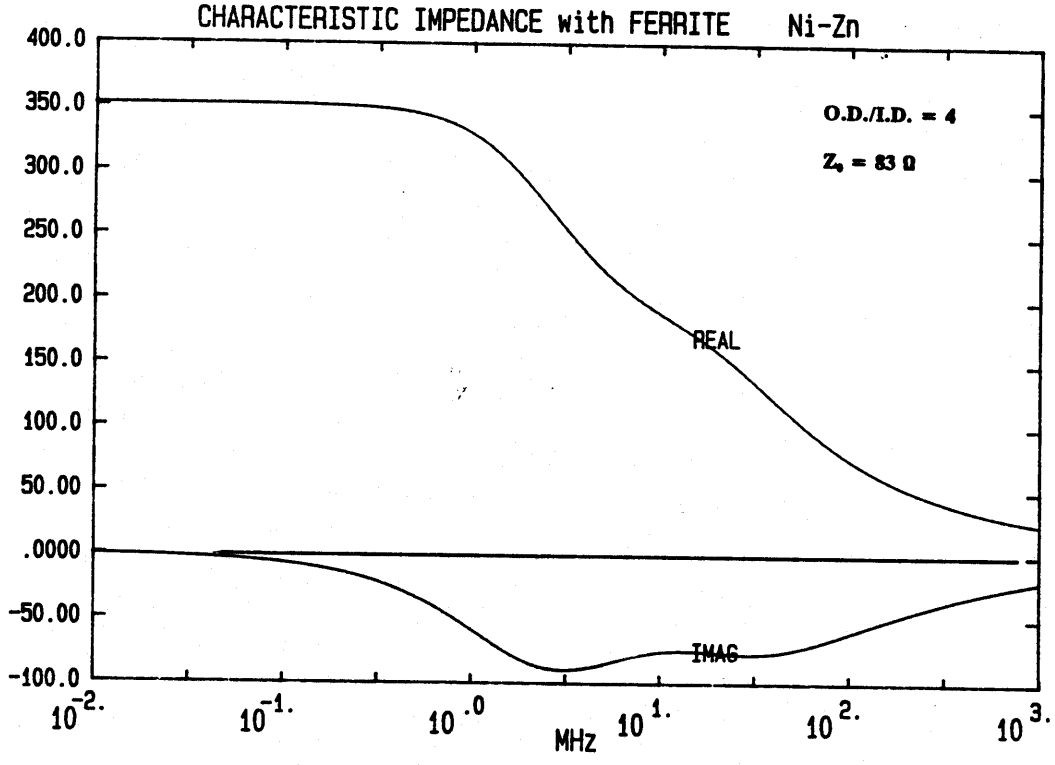

Figure 17. Characteristic Impedance of Line with Ni-Zn Ferrite.

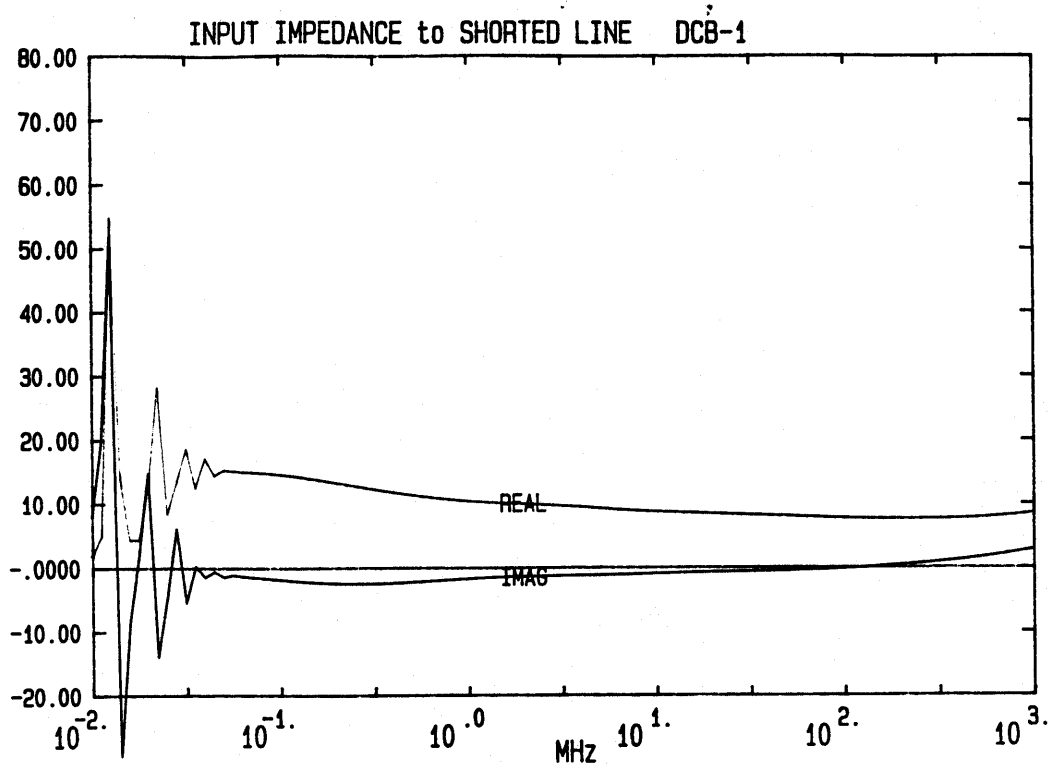

Figure 18. Input Impedance of Mn-Zn Ferrite Line.

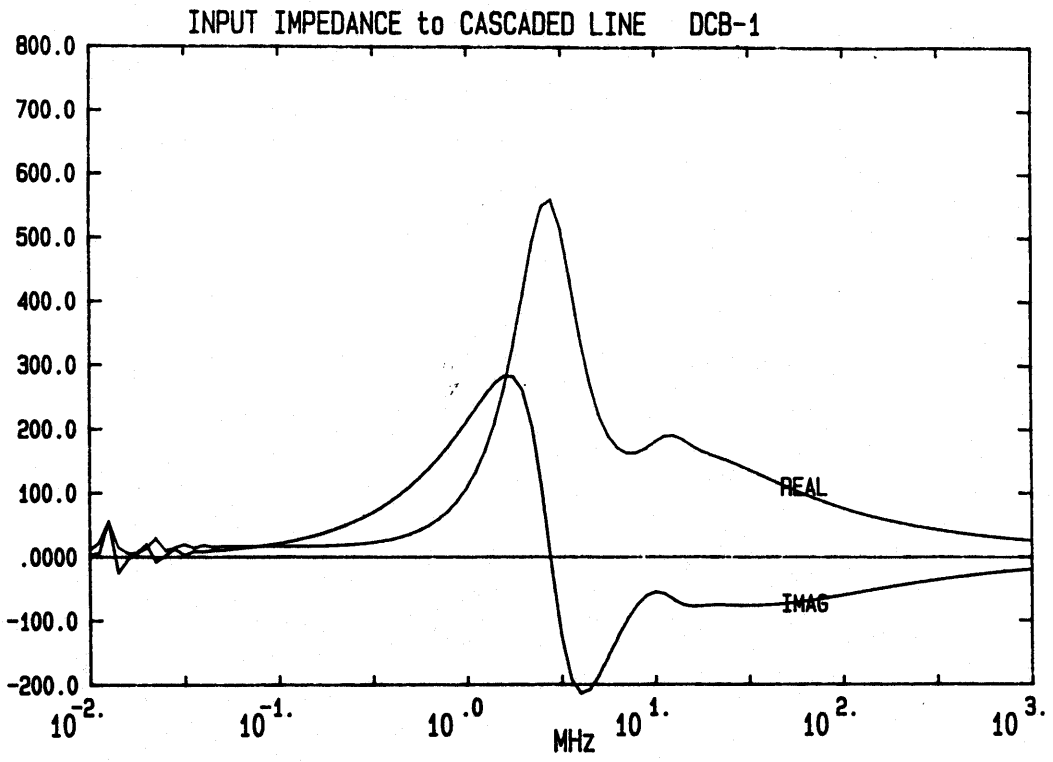

Figure 19. Input Impedance of Cascaded Ni-Zn, Mn-Zn Ferrite Line.

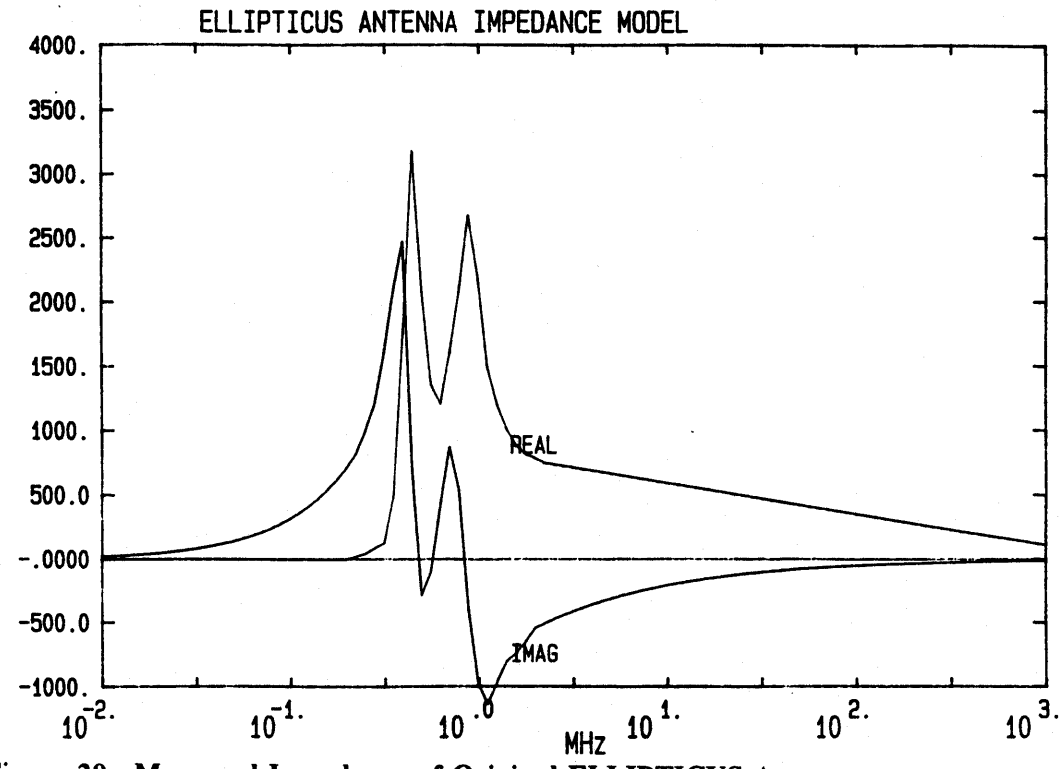

Figure 20. Measured Impedance of Original ELLIPTICUS Antenna.

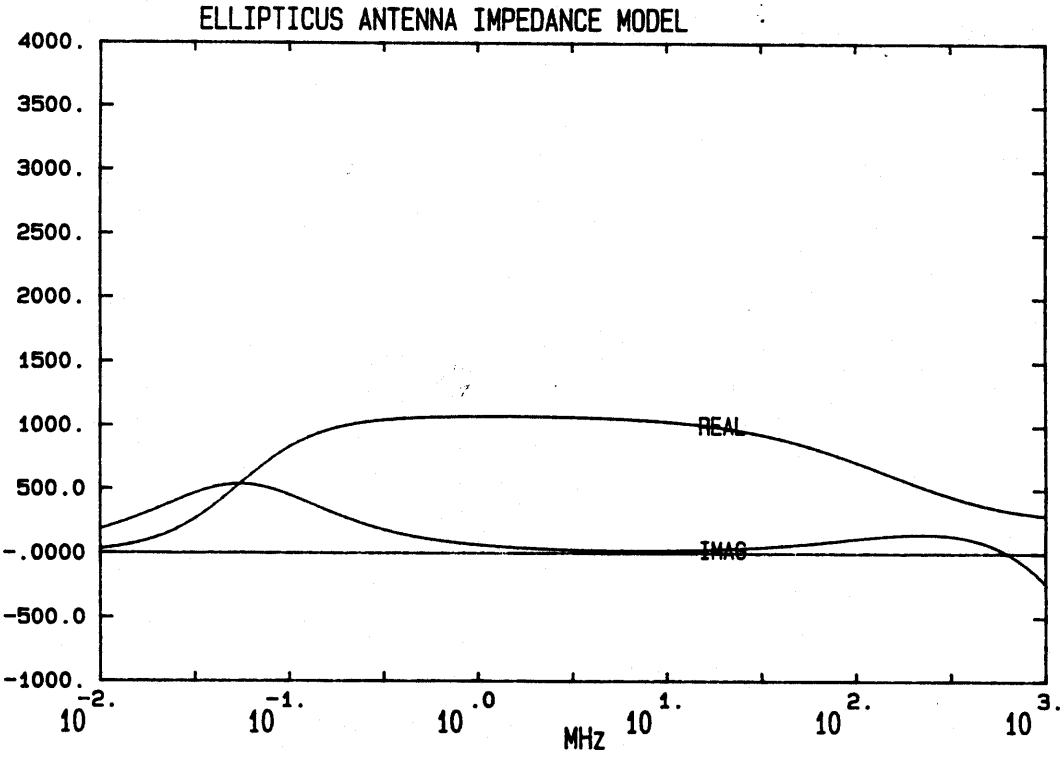

Figure 21. Analytical Model for Ferrite-Loaded Ellipticus Antenna.

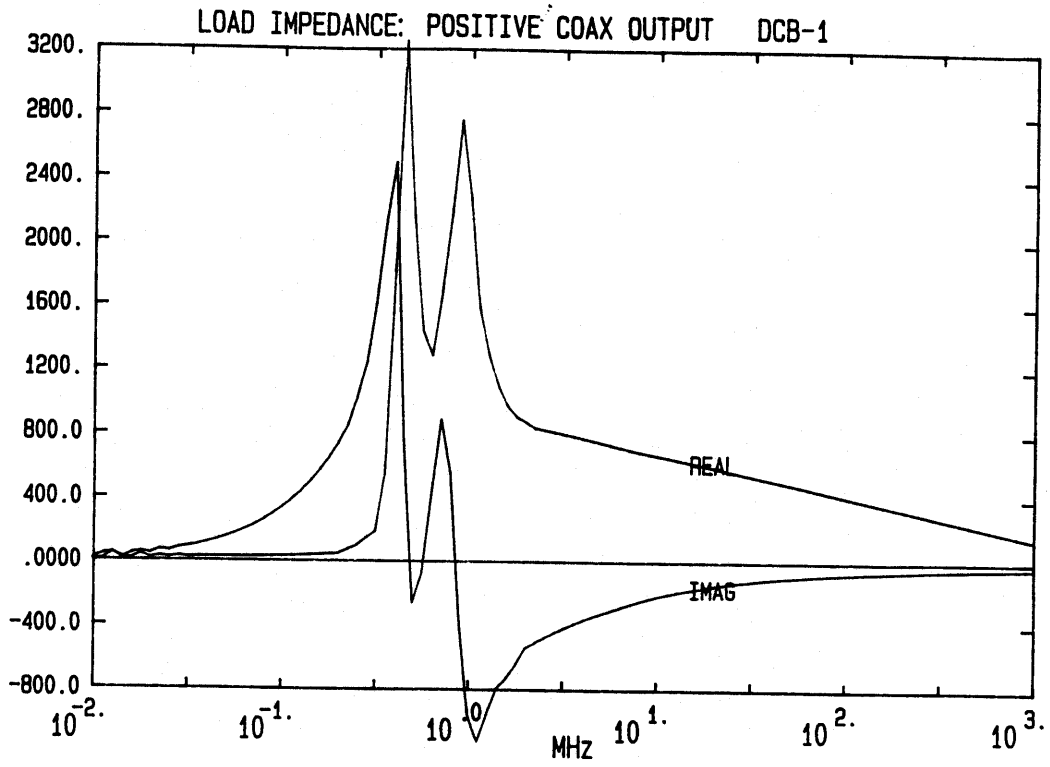

Figure 22. Load Impedance Seen by Positive 100 ohm Coax.

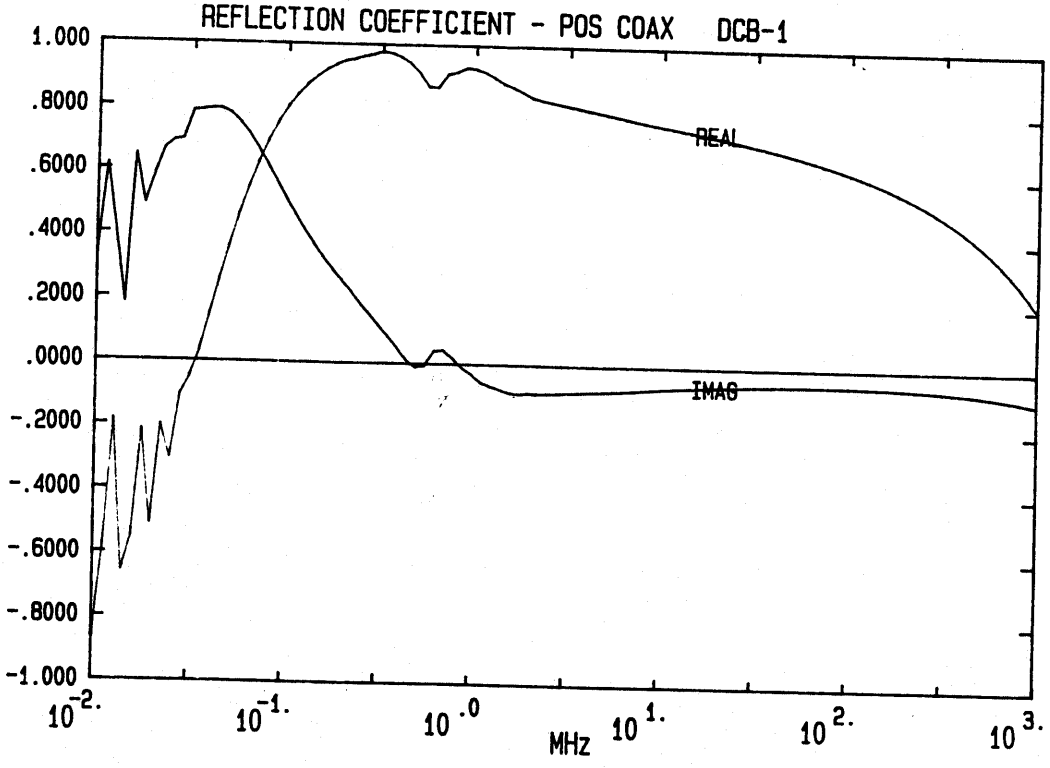

Figure 23. Reflection Coefficient at Positive Coax Output.

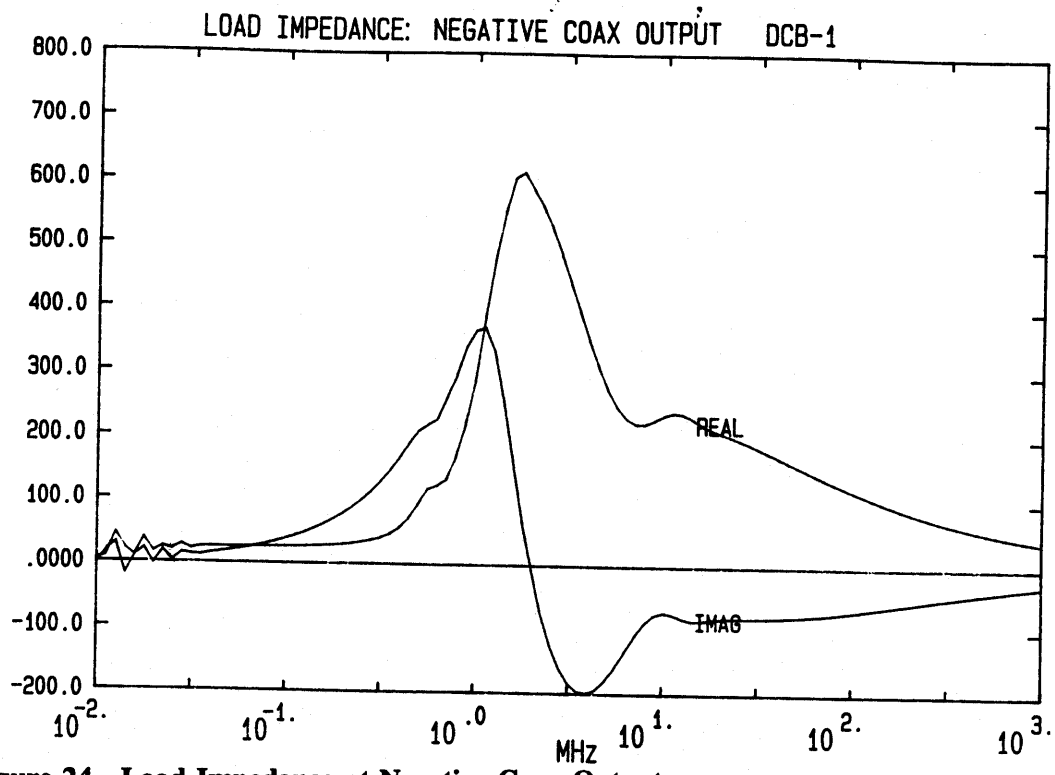

Figure 24. Load Impedance at Negative Coax Output.

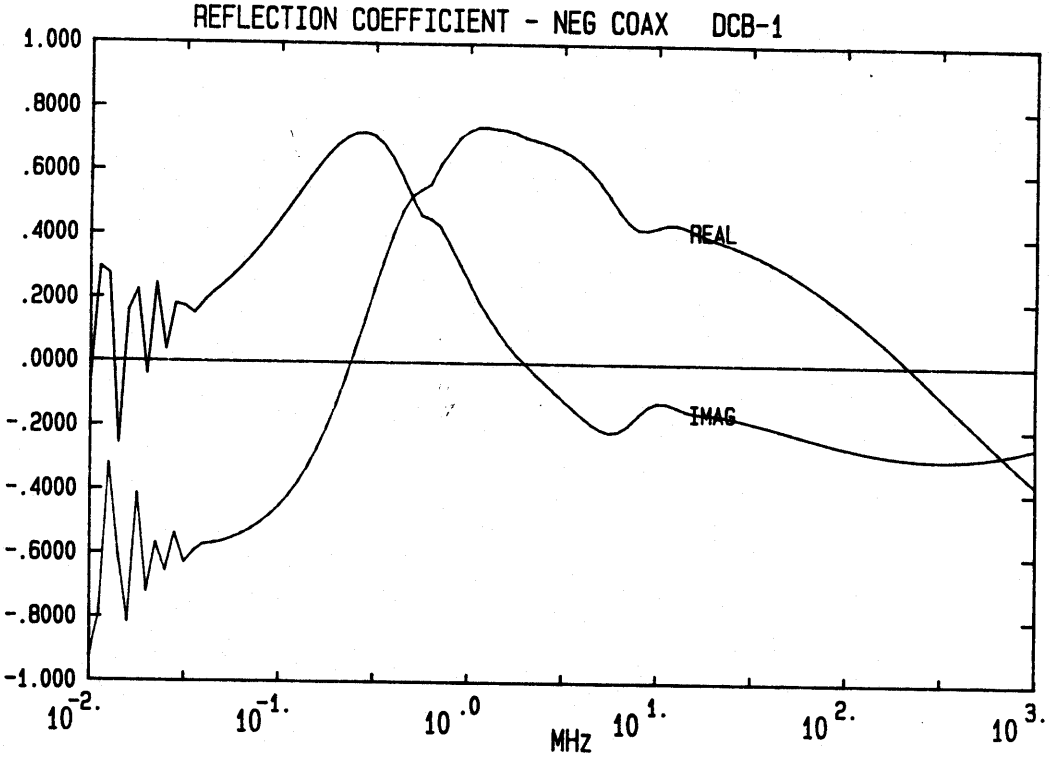

Figure 25. Reflection Coefficient for Negative Coax Output.

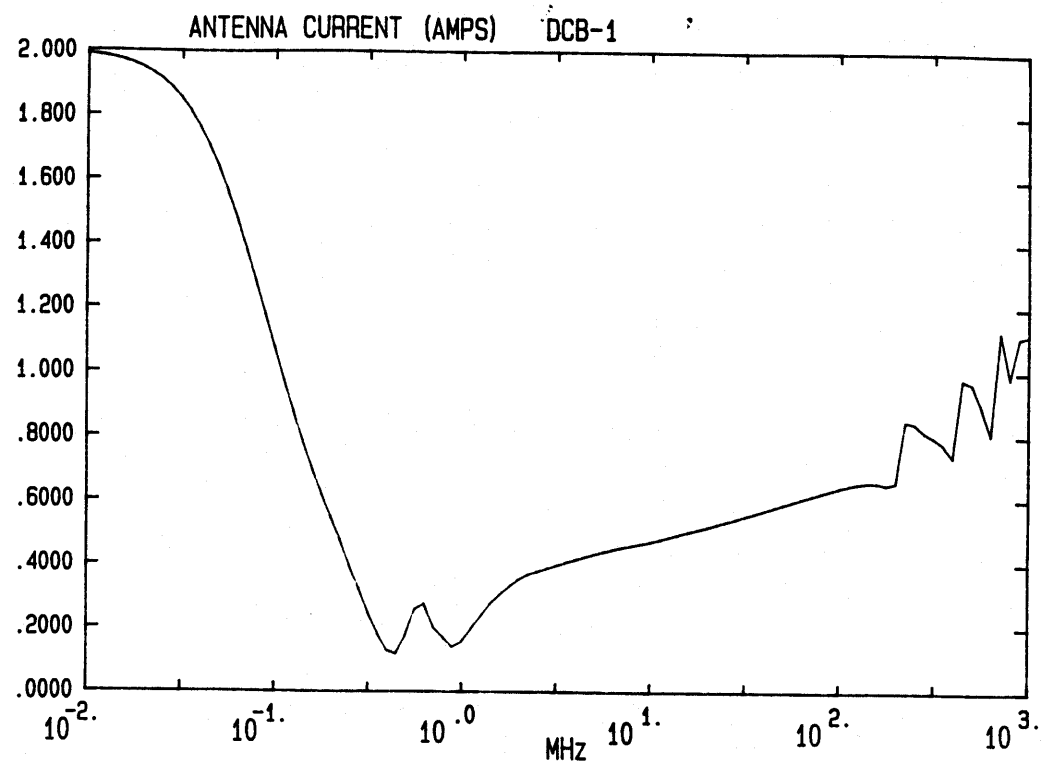

Figure 26. Antenna Current (Old ELLIPTICUS).

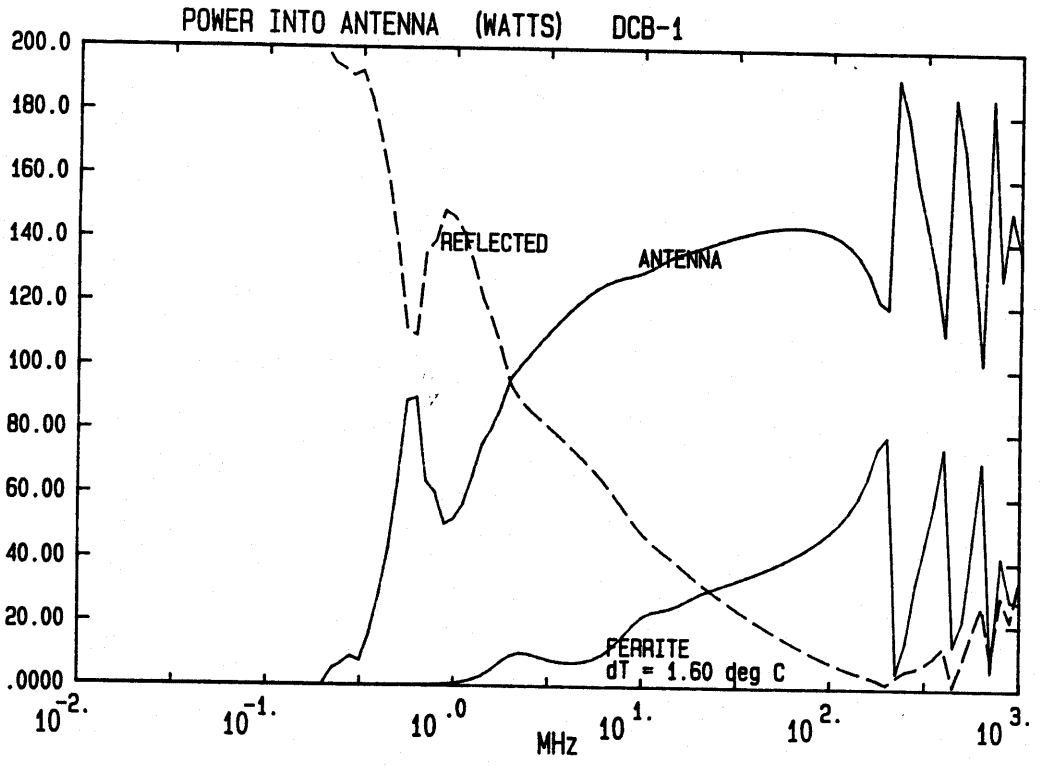

Figure 27. Power into Ferrite, Antenna, and Reflected back into Balun (Old ELLIPTICUS).

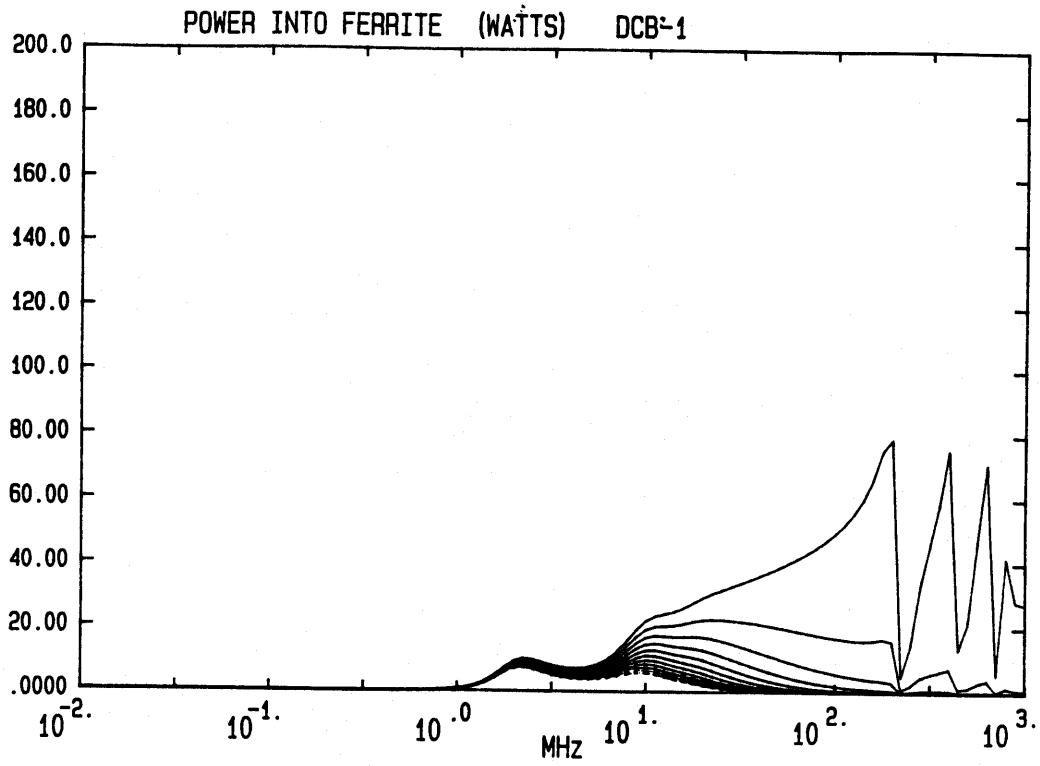

Figure 28. Power Attenuation in Ferrite (1 cm Intervals).

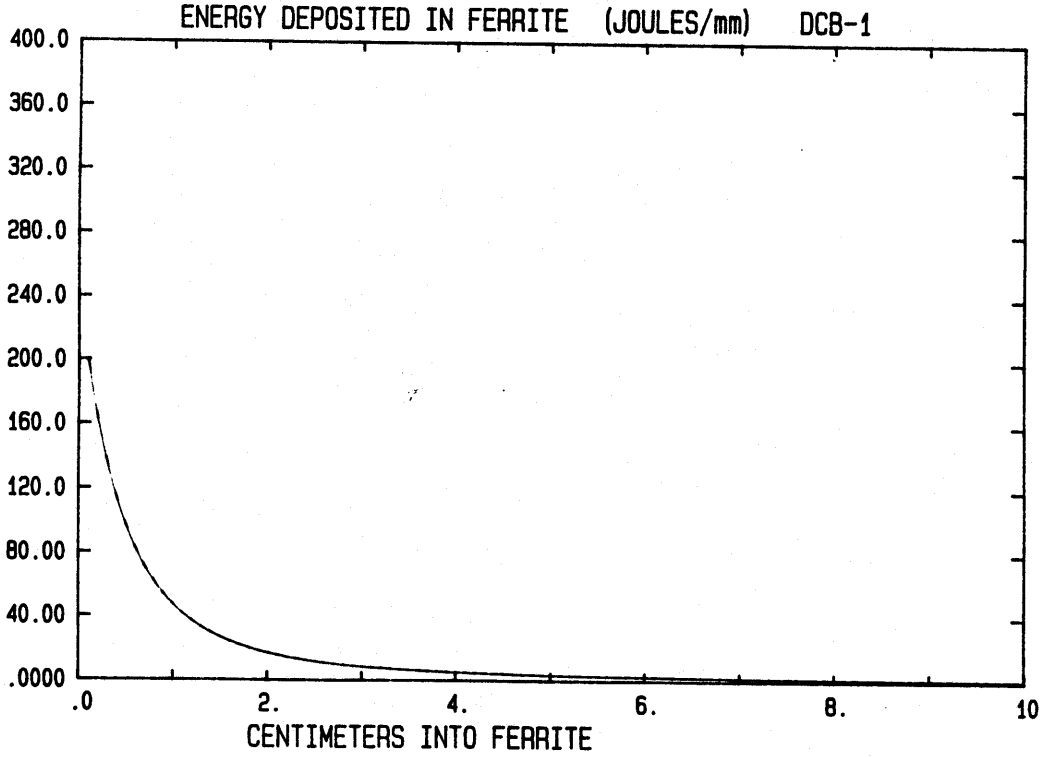

Figure 29. Energy Deposited in Ferrite.

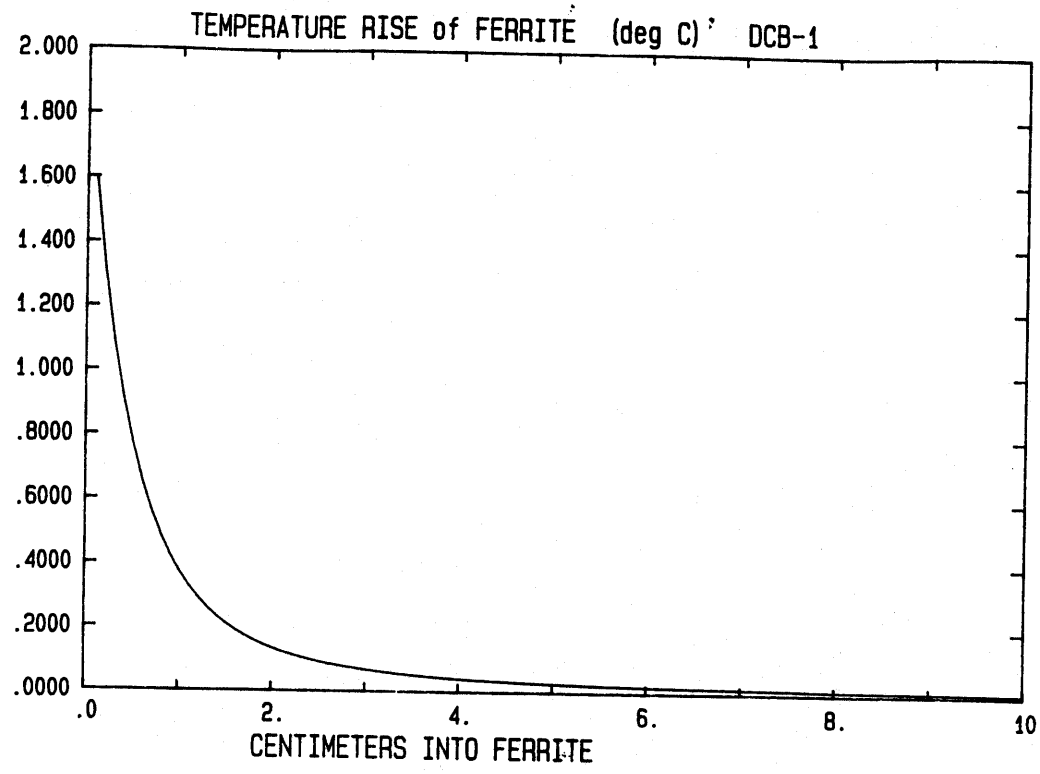

Figure 30. Temperature Rise of Ferrite.

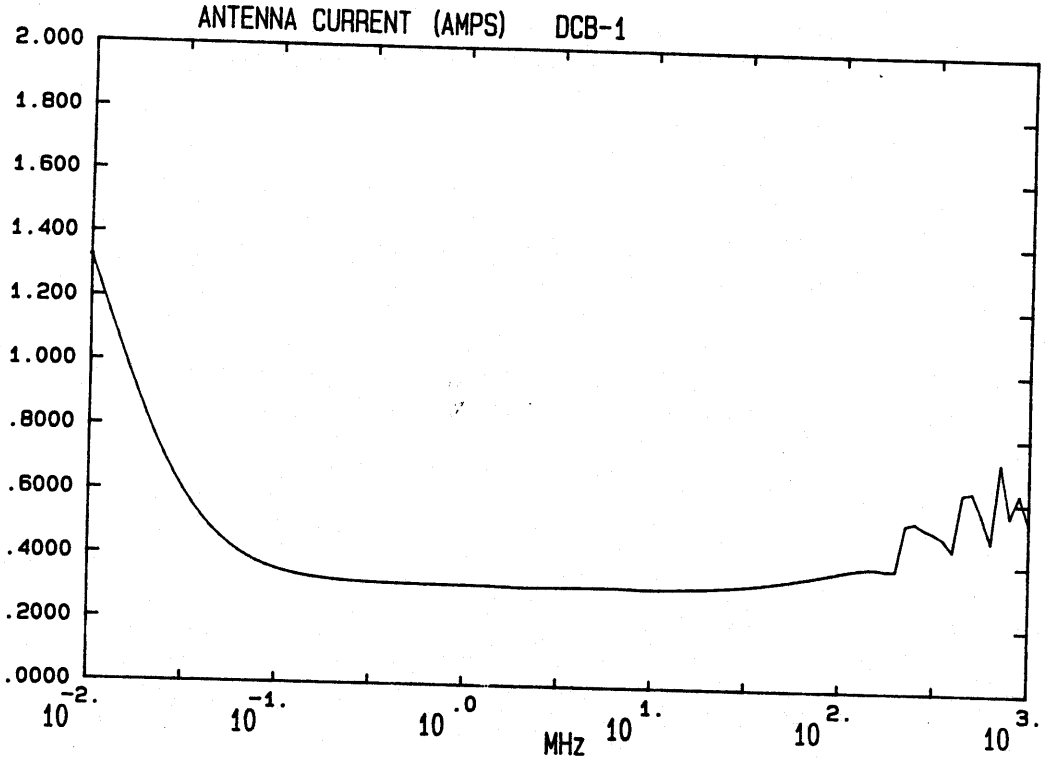

Figure 31. Antenna Current (New ELLIPTICUS Model).

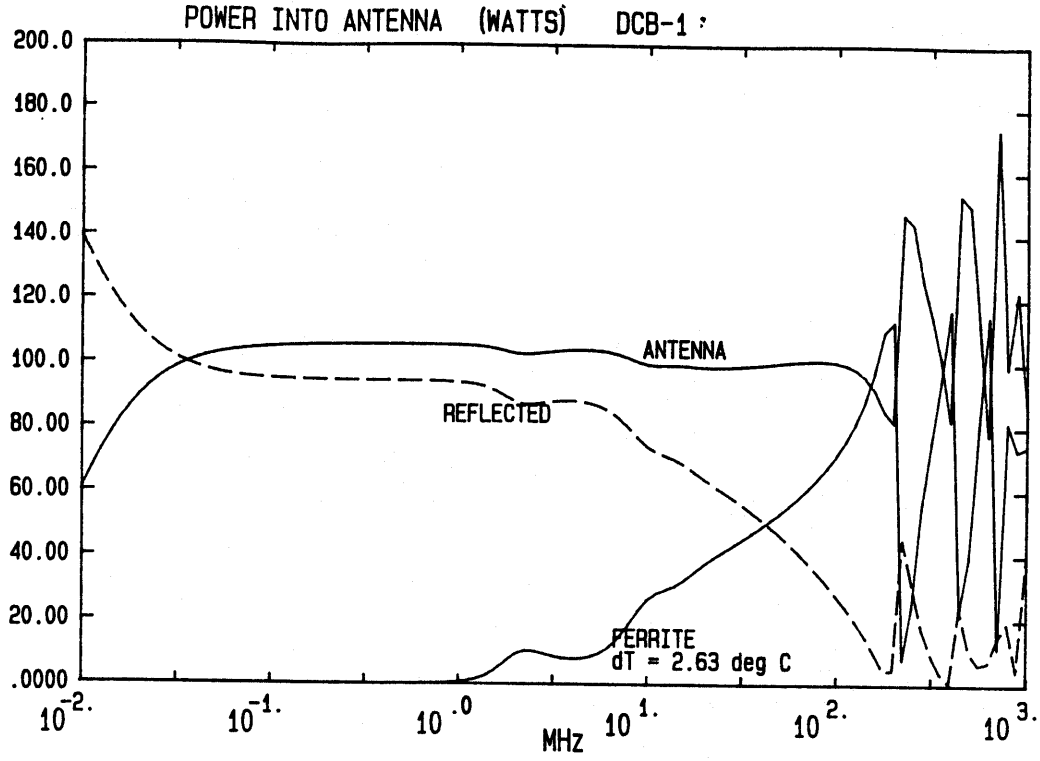

Figure 32. Power into Ferrite, Antenna, and Reflected back into Balun (New ELLIPTICUS Model).

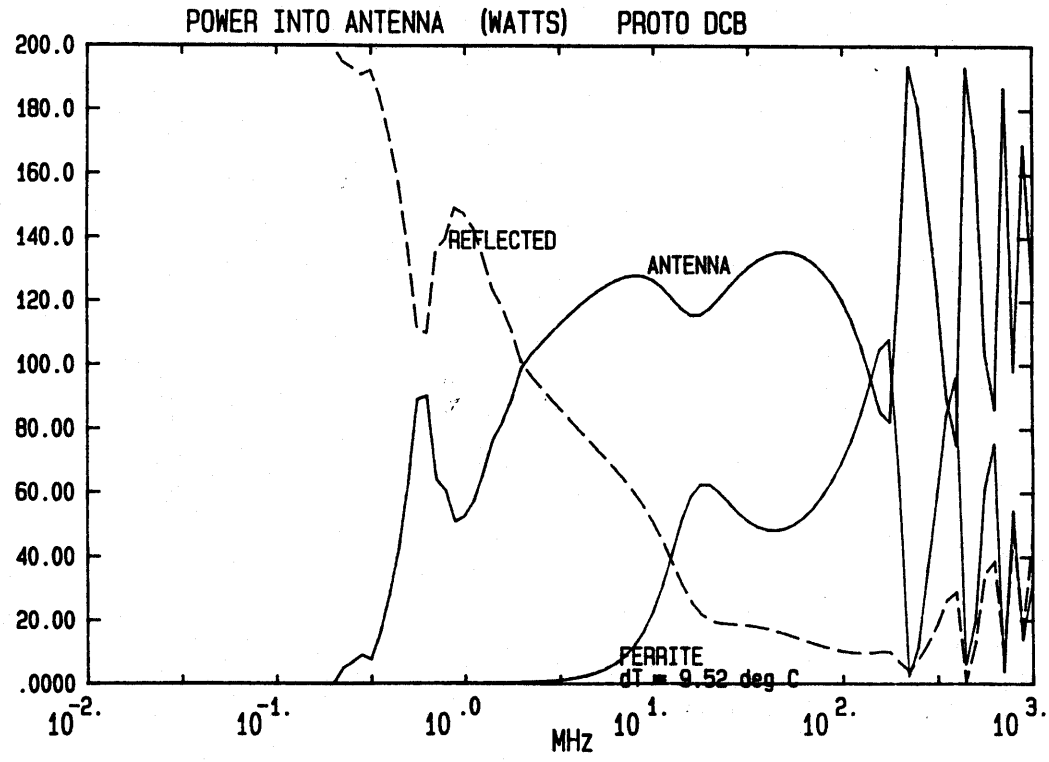

Figure 33. Power Distribution for the Prototype DCB.

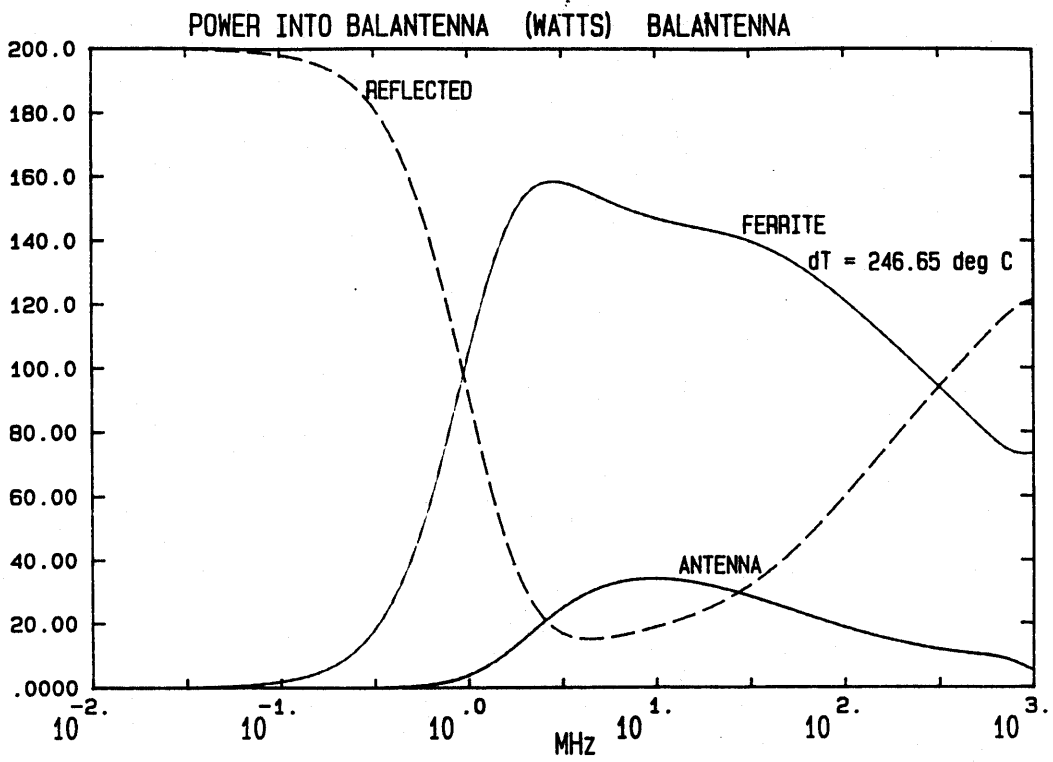

Figure 34. Power Distribution for the Balantenna.

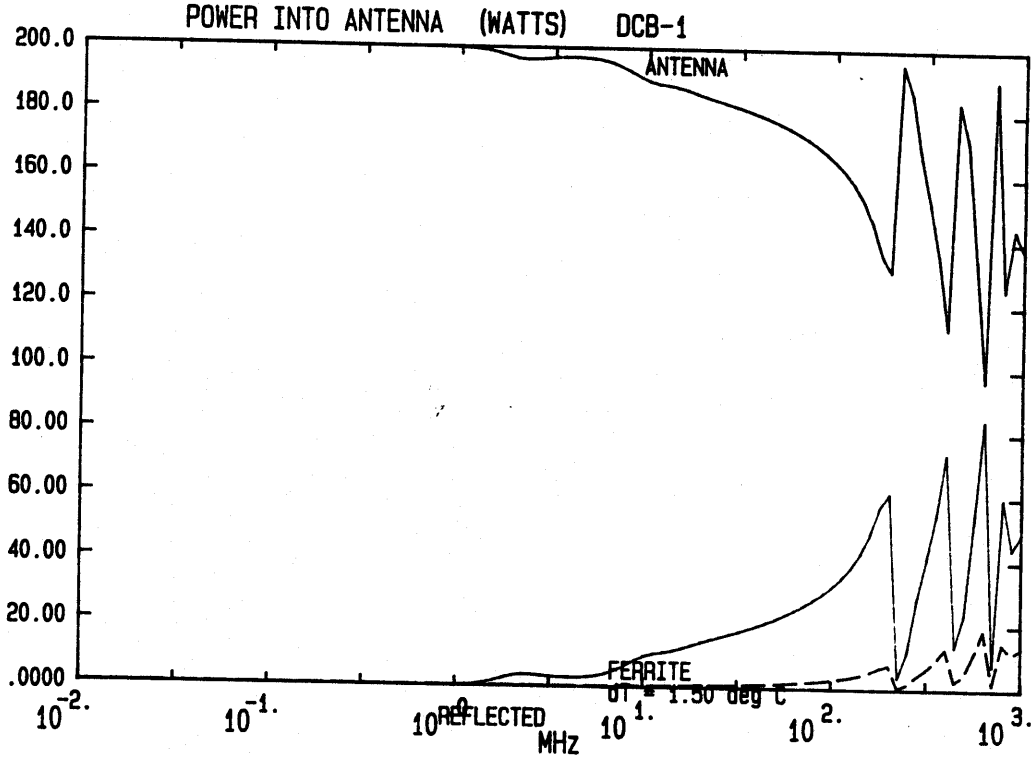

Figure 35. Power Distribution for the DCB-1 (200 ohm load).

REFERENCES

[1] C. E. Baum and D. P. McLemore, "Topology for Transmitting Low-Level Signals from Ground Level to Antenna Excitation Position in Hybrid EMP Simulators," Sensor and Simulation Note 333, Phillips Laboratory, September 1991.

[2] C. E. Baum and D. P. McLemore, "Topology for Transmitting Low-Level Signals from Ground Level to Antenna Excitation Position in Hybrid EMP Simulators," Proceedings 1993 Zurich EMC Symposium, Zurich, Switzerland.

[3] D. P. McLemore, J. Martinez, G. D. Sower, C. E. Baum, T. Tran, and W. D. Prather "The Phillips Laboratory Broadband, High Frequency CW Simulator," National Radio Science Meeting, Boulder, CO, 1993.

[4] G. D. Sower, D. P. McLemore, and W. D. Prather, "Ellipticus Ferrite/Resistive Loading," Measurement Note 41, Phillips Laboratory, February 1993.

[5] G. D. Sower, D. P. McLemore, and W. D. Prather, "Quad Coaxial Balun (QCB)," Measurement Note 44, Phillips Laboratory, August 1993.

[6] D. P. McLemore, G. D. Sower, and C. E. Baum, "The Balantenna: An Integrated Impedance Matching Network and Hybrid EMP Simulator," Sensor and Simulation Note 355, Phillips Laboratory, January 1993.

[7] A. J. Dekker, Solid State Physics, Prentiss Hall, 1962.

[8] P. J. Harrop, Dielectrics, J. Wiley and Sons, New York, 1972, ISBN 0-470-35580-8.

[9] J. Baker-Jarvis, R. G. Geyer, and P. D. Domich, "A Nonlinear Least-Squares Solution with Causality Constraints Applied to Transmission Line Permittivity and Permeability Determination," IEEE Transactions on Instrumentation and Measurement, Vol. 41, No. 5, October 1992.

[10] W. Hartung, D. Moffat, and T. Hays, "Measurements of the Electromagnetic Properties of Some Microwave-Absorbing Materials," SRF-930113/01, Cornell University.

[11] C. E. Baum, "Multiconductor-Transmission-Line Model of Balun and Inverter," Measurement Note 42, Phillips Laboratory, March 1993.